Systematic identification of cancer cell vulnerabilities to natural killer cell-mediated immune surveillance

Matthew F. Pech, Linda E. Fong, Jacqueline E. Villalta, Leanne J.G. Chan, Samir Kharbanda, Jonathon J. O'Brien, Fiona E. McAllister, Ari J. Firestone, Calvin H. Jan, Jeff Settleman[#]

Calico Life Sciences LLC, 1170 Veterans Boulevard, South San Francisco, CA, United States

[#]correspondence: jsettleman@gmail.com

Abstract

Only a subset of cancer patients respond to T-cell checkpoint inhibitors, highlighting the need for alternative immunotherapeutics. We performed CRISPR-Cas9 screens in a leukemia cell line to identify perturbations that enhance natural killer effector functions. Our screens defined critical components of the tumor-immune synapse and highlighted the importance of cancer cell interferon-γ signaling in modulating NK activity. Surprisingly, disrupting the ubiquitin ligase substrate adaptor DCAF15 strongly sensitized cancer cells to NK-mediated clearance. DCAF15 disruption induced an inflamed state in leukemic cells, including increased expression of lymphocyte costimulatory molecules. Proteomic and biochemical analysis revealed that cohesin complex members were endogenous client substrates of DCAF15. Genetic disruption of DCAF15 was phenocopied by treatment with indisulam, an anticancer drug that functions through DCAF15 engagement. In AML patients, reduced DCAF15 expression was associated with improved survival. These findings suggest that DCAF15 inhibition may have useful immunomodulatory properties in the treatment of myeloid neoplasms.

Introduction

Major advances in tumor control have recently been achieved by targeting immune inhibitory signaling pathways. Treatment with "checkpoint inhibitors," antibodies targeting PD1, PD-L1, or CTLA4, lead to durable responses across a wide range of indications, but only in a subset of patients. Treatment response is positively correlated with tumor mutational burden and infiltration of CD8+ effector T cells, which recognize tumor cells via peptides bound to major histocompatibility complex class I (MHC-I) molecules, suggesting that checkpoint inhibitors work best at clearing highly immunogenic cancers with repressed T cell responses [1-3]. Substantial efforts are being made to extend the benefits of immunotherapy to additional patients, including combining checkpoint inhibitors with other therapies, drugging additional lymphocyte-suppressive pathways, and boosting the activity of other arms of the immune system [4].

Resistance to therapy has long been a major problem in cancer treatment. Drugs targeting tumor growth pathways can profoundly reduce tumor burden, but resistance invariably arises, driven by the substantial genetic and phenotypic heterogeneity present within human tumors [5]. Recent clinical and experimental data have similarly highlighted the ability of cancer cells to escape checkpoint inhibitor-induced immune control. B2M and JAK1/2 mutations have been identified in melanoma patients with acquired resistance to checkpoint inhibitors [6,7]. These mutations impair recognition of the tumor by the adaptive immune system, either by directly disrupting antigen presentation or by rendering the cells insensitive to IFNγ, an important inducer of MHC-I expression. Functional genetic screens using T cell-cancer cell cocultures have highlighted similar mechanisms of resistance *in vitro* [8-11]. Even treatment-naïve tumors can be highly immuno-edited, presenting with IFNγ pathway mutations, reduced MHC-I expression and loss of the peptide sequences that can serve as antigens [12-15]. Together, these findings highlight a critical need for therapies that can either increase MHC expression or work in a MHC-independent fashion.

Anti-tumor immunity is not solely mediated by the adaptive immune compartment. Innate immune cells, most notably natural killer (NK) cells, can have both direct tumoricidal activity and also help to fully elaborate long-lasting anti-tumor responses [16-19]. NK cells are cytotoxic lymphocytes capable of mounting rapid responses to damaged, infected, or stressed cells, including cancer cells.

T and NK cells share effector functions, releasing cytokines and exocytosing lytic granules upon activation to kill target cells. However, NK activation status is controlled by the integrated signals from germline-encoded NK-activating and -inhibiting receptors (aNKRs/iNKRs). Generally, iNKR ligands are expressed by normal and healthy cells, whereas aNKR ligands are upregulated after DNA damage or viral insult [19,20]. MHC-I molecules provide a potent inhibitory signal sensed by NK cells, enabling the innate immune system to respond productively to MHC-deficient cells. As a result, there is considerable interest in amplifying NK responses to cancers, as well as developing NK-based cell therapies [18-20].

Here, we performed genetic screens in an MHC-deficient leukemic cell line to systematically identify modulators of NK-mediated anti-cancer immunity. These screens, unexpectedly, revealed the potential therapeutic utility of targeting the CRL4 substrate adaptor DCAF15 in myeloid malignancies. Disruption of DCAF15 strongly sensitized cancer cells to NK-mediated killing, resulting from increased cancer cell expression of lymphocyte costimulatory molecules. Proteomic experiments revealed that DCAF15 interacted with and promoted the ubiqitination of the cohesin complex members. Treatment with indisulam, an anticancer drug that modulates DCAF15 function, reduced interaction with cohesin members and mimicked DCAF15 loss-of-function immunophenotypes.

Results

A genome-scale CRISPR screen identifies modulators of NK effector functions

We performed genome-scale CRISPR screens in K562 cells to identify perturbations that modulate NK-92-mediated killing (Figure 1A). K562 human chronic myelogenous leukemia cells are a NK-sensitive cancer cell line that weakly expresses MHC-I. For screening purposes, a clonal isolate of K562 cells expressing high levels of spCas9 was generated and validated (Figure 1- figure supplement 1A-C). NK-92 cells are a human lymphoma-derived cell line phenotypically similar to activated NK cells.[21] These cells exhibit interleukin-2 (IL-2)-dependent growth, express a large number of aNKRs and few iNKRs [22], and display potent cytolytic activity against K562 cells.

In pilot experiments, labeled K562 cells were co-cultured with NK-92 cells to determine an effector-to-target (E:T) ratio that applied sufficient selective pressure for screening (Figure 1-figure supplement 1D-F). IL-2 was removed during the co-culture to promote the eventual death of NK-92 cells, allowing the collection of genomic DNA preparations undiluted by effector cell DNA. A multi-day timeframe between the NK-92 challenge and screen readout was used to capture tumor cell fitness changes related both to the direct cytolytic activities of NK cells as well as the longer-term effects from NK-released cytokines.

For the co-culture screen, cas9-expressing K562 cells were infected with a genome-scale single guide RNA (sgRNA) library targeting all unique coding genes and miRNAs, as well as one thousand non-targeting controls (Table S2). Seven days post-infection, cells were either grown normally or challenged with NK-92 cells at a 1:1 or 2.5:1 E:T ratio, reducing K562 cell counts 19-fold or 43-fold, respectively, by the end of the screen (Figure 1B). Deep sequencing was used to compare changes in sgRNA abundance between the challenged and unchallenged state after 8 days of co-culture, and genes were ranked using the MAGeCK software [23]. (Figure 1C, Table S2) There was good agreement between the results from screens performed at the different E:T ratios (Figure 1- figure supplement 2).

The screen revealed two broad classes of "hits"— sgRNAs targeting components of the tumor-immune synapse or components of the IFNγ signaling pathway (Figure 1C-D). Disruption of ICAM1 was the top-ranked NK-92 evasion mechanism, scoring many orders of magnitude stronger than any other gene—an observation consistent with the critical role of ICAM1-LFA1 interactions in establishing initial target-lymphocyte adhesion and polarizing cytotoxic granules towards the synapse [16]. Single guide RNAs targeting multiple other tumor-immune synapse components were also enriched after NK-92 challenge, including NCR3LG1 (#26-ranked gene by MaGeCK score), the activating ligand for NKP30 on NK cells [24]; CD58 (#37), an adhesion molecule that binds CD2 [25,26] ; and CD84 (#80), a SLAM-related receptor that binds homotypically to promote activation and cytokine secretion in lymphocytes [27-29]. Other than NECTIN2, sgRNAs targeting NK-inhibitory surface proteins did not score prominently as NK-sensitization mechanisms, consistent with the weak MHC-I expression on K562 cells and the limited repertoire of NK inhibitory receptors expressed on NK-92 cells [22]. NECTIN2 transmits both stimulatory or

inhibitory signals to NK cells, depending on whether it is bound to DNAM1 (CD226) or TIGIT, respectively [30,31].

After ICAM1, the top 10 highest scoring NK-92 evasion mechanisms were dominated by sgRNAs targeting the proximal components of the IFNγ signaling pathway, including STAT1, JAK1, IFNGR2, JAK2 and INFGR1 (Figure 1D). Consistent with the importance of cancer cell IFNγ signaling, sgRNAs targeting negative regulators of the interferon response were strongly depleted after NK-92 challenge. Disruption of the protein tyrosine phosphatases PTPN2 and PTPN1 were the #2 and #5 ranked NK-92 -sensitizing mechanisms, respectively. Presumably, these proteins suppress IFNγ-induced immunomodulation by dephosphorylating STAT and JAK proteins, as has been reported in CRISPR screens using T-cell coculture systems or syngeneic tumor models [9,10]. Taken together, these findings indicate that our *in vitro* functional genomics screens effectively revealed known components of physiologically-relevant immune synapse and cytokine pathways.

Prospective identification of novel genes affecting sensitization to NK cells

Mechanisms of NK-92 sensitization identified in the screen were diverse, revealing many strongly-scoring genes not previously linked to either interferon signaling or NK cell biology (Figure 1). Most surprisingly, the top-ranked mechanism for promoting NK-92 mediated clearance was disruption of DCAF15, an uncharacterized substrate adaptor for CRL4 ubiquitin E3 ligases. DCAF15 is a member of the large family of DDB1 and Cul4-associated factors (DCAFs) [32]. CRL4 complexes enable cells to mark proteins for proteosomal degradation, helping regulate intracellular protein homeostasis. As substrate adaptors for CRL4, DCAF proteins provide specificity to the complex, determining which client proteins are ubiquitinated [33]. As with most substrate adaptors, the normal client repertoire of DCAF15 is undefined, and relatively little is known about the biological function of DCAF15.

We also noted that disruption of two cohesin-related genes, STAG2 and HDAC8, scored as NK-92 sensitization factors (ranked #26 and #19, respectively). Cohesin is a ring-shaped complex involved in chromatin replication, organization and repair, with STAG2 acting as a core complex member and HDAC8 controlling chromatin accessibility [34]. Cohesin dysregulation has cell

context-specific consequences, including DNA damage and aneuploidy; in leukemic cells, cohesin mutations are thought to enforce stem cell programs by altering chromatin organization [35].

A phenotypic screen based on MHC-I upregulation to identify modulators of the IFNγ response

The prominent role for IFNγ signaling in the immune response to cancer cells, both clinically and in our screens, prompted us to define more specifically which NK-92-sensitizing genes are involved in modulating the IFNγ response. MHC-I levels are highly upregulated in K562 cells after IFNγ exposure, increasing 5.9+/-0.98 fold after 24hrs of exposure to IFNγ. This induction was dependent on STAT1 and was nearly doubled by disrupting PTPN2 (Figure 2A-B and Figure 2- figure supplement 1). We therefore used IFNγ-induced cell surface MHC-I expression as a proxy for the strength of the interferon response. K562 cells transduced with a genome-scale CRISPR library were treated with IFNγ for 24hrs and MHC-I expression was measured by flow cytometry. The brightest 20% and dimmest 20% of cells were sorted, and deep sequencing was used to compare sgRNA abundance between the populations (Figure 2C, Table S3).

As expected, cells with impaired MHC-I upregulation were highly enriched for sgRNAs targeting the IFNγ-JAK-STAT pathway (IFNGR1/2, JAK1/2, STAT1, IRF1/2), as well as the antigen processing/presentation machinery (B2M, TAP1/2, TAPBP, PDIA3, HLA-C/B) (Figure 2D). Conversely, disruption of PTPN2 or STAG2 induced an exuberant MHC-I response. Surprisingly, sgRNAs targeting epigenetic factors were highly enriched within the brightest MHC-I expressing cells—most prominently, members of the BCOR complex PCGF1 and KDM2B, members of the PRC2 complex EZH2 and SUZ12, as well as factors affecting histone methylation/acetylation status.

Rank-rank comparisons between the NK and MHC screens were informative in prospectively defining a core group of IFNγ response genes in K562 cells (Figure 2E). Comparing sgRNAs enriched after NK-92 challenge with those causing impaired MHC-I upregulation clearly delineated the known proximal components of the IFNγ signaling pathway (IFNGR1/2, JAK1/2,

STAT1), and highlighted several poorly characterized genes such as GSE1, SPPL3 and NR2F2 (Figure 2E).

Surprisingly, comparing sgRNAs depleted after NK-92 challenge with those causing an exaggerated MHC-I response highlighted the CRL4 substrate adaptor DCAF15 most prominently, alongside the cohesin members STAG2 and HDAC8 (Figure 2E). As expected, negative feedback regulators of the IFNγ pathway (PTPN1 and PTPN2) were also recovered by this analysis. We focused additional studies on understanding the function of DCAF15, given its prominence in both the NK sensitization (#1 ranked hit at 2.5 E:T ratio; #12 ranked hit at 1:1 E:T ratio) and MHC upregulation (#13 ranked hit) screens.

Disruption of DCAF15 enhances NK effector functions

To evaluate hits from the CRISPR screens, we generated individual gene knockout (KO) cell lines by lentiviral sgRNA expression, producing polyclonal cell lines with high levels of gene disruption (Figure 2- figure supplement 1 and Figure 3-figure supplement 1). Fluorescently-labeled control or test KO target cell lines were subjected to competitive co-culture assays in the presence of either NK-92 or primary NK effector cells, with changes in the relative ratios of target cell types measured over time by flow cytometry (Figure 3A).

As expected, disrupting ICAM1 in K562 cells conferred very high levels of protection against NK-92 cells (Figure 3B-C; 19.7-fold enrichment). Disabling signaling downstream of IFNγ by disrupting STAT1 provided an intermediate level of resistance (2.45-fold enrichment). K562s are very sensitive to NK-mediated killing, providing a large dynamic range for detection of resistance-promoting factors, while limiting the ability of the assay to detect similarly large increases in sensitization. Nevertheless, multiple independent sgRNAs targeting DCAF15 promoted sensitization to NK-92 cells (1.6-fold depletion), with a similar degree of preferential killing observed for NECTIN2 or PTPN2 KO cells (NECTIN2: 1.95-fold depletion; PTPN2: 1.4-fold depletion).

We repeated NK-92 competitive co-culture experiments after disruption of DCAF15, PTPN2, STAT1 and ICAM1 in Daudi cells, a B2M-deficient B-cell lymphoma line (Figure 3D, Figure 3-figure supplement 1D-F). ICAM1 KO Daudi cells were highly protected against NK-92 cell killing, whereas disruption of DCAF15 or PTPN2 led to enhanced killing. In contrast to K562 cells, STAT1 disruption in Daudi cells promoted their preferential killing.

To extend these observations to primary NK cells, human peripheral NK cells were isolated from PBMCs of 6 healthy donors, activated and challenged in competitive co-cultures with various K562 KO cell genotypes (Figure 3E and Figure 3- figure supplement 2). Disruption of DCAF15 or PTPN2 promoted sensitization to primary NK cells, albeit with reduced magnitudes of effect compared to NK-92 cells (PTPN2: 1.3-fold depletion; DCAF15: 1.15-fold depletion). In 3 out of 6 donors, NK cells showed increased degranulation, as measured by cell surface CD107a expression, when challenged with DCAF15 KO cells (Figure 3F). ICAM1 disruption promoted resistance to NK cell attack, but only conferred partial protection (2.3-fold enrichment). The effect of STAT1 disruption was extremely variable, with STAT1 KO K562 cells strongly preferentially killed by primary NK cells from a subset of donors. These findings implicate DCAF15 and PTPN2 as novel modulators of NK-mediated cancer cell immunity.

Loss of the cullin-RING E3 ligase substrate adaptor DCAF15 leads to an inflamed state distinct from dysregulated IFNγ signaling

DCAF15 was a strong hit in both the NK sensitization and MHC upregulation screens, suggesting that DCAF15 disruption sensitizes K562 cells to NK-mediated killing by dysregulating the IFNγ response. Consistent with the screening results, polyclonal K562 cells expressing DCAF15 sgRNAs ("DCAF15 KO cells") displayed 2.45-fold higher levels of MHC-I than control knockout cells after 24hrs of IFNγ exposure, an effect comparable in magnitude to PTPN2 disruption (Figure 4A). We then tested whether DCAF15 KO cells exhibited hallmarks of dysregulated JAK-STAT signaling, using PTPN2 KO cells as a positive control. We were unable to see any difference in induction of STAT1 phosphorylation after IFNγ exposure in DCAF15 KO cells, or differences in steady state levels of STAT1/2, JAK1/2 or IFNGR1 (Figure 4B and data not shown). DCAF15 KO cells appeared healthy and proliferated at a normal rate (Figure 4 – figure supplement S1A). As in

wild-type K562 cells, long-term IFNγ exposure was neither cytotoxic nor cytostatic to DCAF15 KO cells (Figure 4c and [36]). In contrast, PTPN2 KO cells showed higher levels of $STAT1^{PY701}$ induction after IFNγ exposure, and their proliferative rate was temporarily reduced after transient exposure to IFNγ, or more substantially slowed down by continuous treatment with the cytokine (Figure 4B-C).

We explored the transcriptional and immunophenotypic response of cells to IFNγ treatment. RNA-seq and flow cytometry was performed on control, DCAF15 KO or PTPN2 KO K562 cells basally and after 24hrs of IFNγ exposure. Wild-type cells dramatically upregulated transcription of anti-viral genes and components of the antigen processing and presentation pathway after IFNγ treatment (Figure 4 – figure supplement 1B and Table S4). On the cell surface, K562 cells exhibited STAT1-dependent upregulation of ICAM1 expression after IFNγ treatment, with a variety of other important NK ligands unaffected by cytokine treatment (Figure 4- figure supplement 1C).

Clustering analysis clearly showed that PTPN2 KO cells were transcriptionally distinct from control or DCAF15 KO cells both before and after cytokine exposure (Figure 4D). In the basal state, PTPN2 KO cells were enriched for inflammation and interferon-associated Gene Ontology (GO) terms (Figure 4 – figure supplement 1D). After cytokine exposure, gene set enrichment analysis revealed that PTPN2 KO cells had exaggerated transcriptional responses to interferon and were also enriched for apoptotic GO gene categories (Figure 4 – figure supplement 1E). PTPN2 KO cells also showed greater IFNγ-induced MHC-I and ICAM1 cell surface expression (Figure 2A and Figure 4 – figure supplement 1C). These results suggest that loss of appropriate IFNγ negative feedback may both promote cell death and modulate NK cell interactions.

In contrast, DCAF15 KO cells did not show substantial differences in their transcriptional response to IFNγ (Figure 4D). However, DCAF15 KO cells were enriched for GO terms associated with NK-mediated cytotoxicity, antigen presentation and cell adhesion, consistent with our phenotypic characterization of these cells (Figure 4E). Together, these findings indicate that while DCAF15

KO K562 cells exhibit a relatively normal response to IFNγ stimulation, they are nonetheless in an inflamed state primed to interact with cytotoxic lymphocytes.

DCAF15 knockout cells enhance NK-92 triggering via CD80 expression

Intriguingly, differential expression analysis showed that one of the most significantly upregulated genes in DCAF15 KO K562 cells was CD80 (Figure 4F; Q value 3.7e-23, Beta value 0.98). CD80 is an important co-stimulatory molecule for lymphocytes, regulating T cell activation and tolerance by ligation to CD28, CTLA4 or PDL1 [37]. During antigen-presenting cell (APC) activation, the upregulation of MHC molecules and CD80 provide critical antigenic and costimulatory signals to T cells [38]. K562 cells are an undifferentiated and multipotential CML cell line, well-studied for their ability to differentiate towards many different lineages, including APC-like states [39]. We hypothesized that upregulation of MHC-I and CD80 in DCAF15 KO cells may reflect a broader acquisition of APC-like properties. Indeed, immunophenotyping of unstimulated DCAF15 KO cells revealed higher levels of the APC markers CD80, CD40 as well as class I and II MHC molecules (Figure 5A; 2.23-fold CD80 increase; 2.01-fold CD40 increase; 1.44-fold MHC-I increase; 1.22-fold MHC-II increase). DCAF15 KO cells did not display higher levels of the APC maturation marker CD83 (Figure 5A). Expression levels of B7H6, ICAM1, ULBP2/5/6, IFNGR1, CD58 and NECTIN2 were either unaltered in DCAF15 KO cells or modestly changed in a fashion not expected to increase sensitivity to NK cells (Figure 5 – figure supplement 1A). Importantly, the changes to the DCAF15 KO cell immunophenotype could be rescued by constitutive expression of a sgRNA-resistant DCAF15 open-reading frame (Figure 5 – figure supplement 1B-D).

Transducing tumors with the B7 ligands CD80 or CD86 can enhance anti-tumor immunity by enabling the tumor cells to directly deliver antigenic and costimulatory signals to T and NK cells [40-43]. While best understood in the context of T cell biology, B7 ligands have been shown to promote NK activation, via CD28-dependent and -independent pathways [42-46]. We confirmed that NK-92 cells are CD28-positive, whereas we could not detect CD28 on peripheral CD3- CD56+ NK cells (Figure 5 – figure supplement 1E-F). K562 cells stably over-expressing wild-type CD80 were generated (Figure 5B; 49-fold higher CD80 levels than endogenous). Over-expression was

sufficient to increase K562 sensitivity to NK-92 mediated killing (Figure 5C), whereas overexpression of a mutant form of CD80 carrying point mutations that abrogate CD28 binding [47] ($CD80^{Q65A,M72A}$) had no effect.

We next determined whether the increased CD80 expression in DCAF15 KO cells was important for their altered NK-92 sensitivity. Changes in NK-92 degranulation were measured after incubation with K562 cells pretreated with either control or CD80 blocking antibodies (Figure 5D). As expected, ICAM1 KO cells triggered less NK-92 degranulation than control cells (by 52±12%) and were not significantly affected by CD80 antagonism (Figure 5E). DCAF15 KO cells showed a 17±8% increased ability to trigger NK-92 cells and were approximately twice as sensitive to CD80 antagonism compared to control cells (Figure 5E-F). Following CD80 antagonism, degranulation triggered by DCAF15 KO was not significantly different from untreated control cells. Taken together, these results indicate that DCAF15 disruption in K562 cells induces an APC-like immunophenotype conducive to promoting lymphocyte responses, with higher CD80 expression especially important for increased NK-92 cell triggering.

The anti-leukemia drug indisulam inhibits DCAF15 function

Aryl sulfonamide drugs have demonstrated promising anti-cancer properties in hematological malignancies [48]. Recently, it was discovered that these agents work by binding DCAF15 and redirecting the ubiquitination activity of the CRL4-DCAF15 E3 ligase towards the essential splicing factor RBM39 [49,50]. This mechanism of action is conceptually similar to that of the "IMiD" thalidomide analogs, which promote the degradation of various lymphocyte transcription factors by engaging the CRL4-cereblon E3 ubiquitin ligase [51-53]. Presumably, sulfonamides and IMiDs also impair the degradation of the normal client proteins when they induce neomorphic activity of the substrate adaptor. This has not been proven, however, as it is difficult to systematically determine the normal substrate repertoire of adaptor proteins.

We hypothesized that treating cells with low concentrations of the aryl sulfonamide indisulam would phenocopy DCAF15 depletion (Figure 6A). Three-day dose-response experiments revealed that K562 cells were sensitive to indisulam, and that DCAF15 disruption reduced this sensitivity,

consistent with previous reports[50] (Figure 6B). Dose-response experiments across a panel of 16 hematological cancer cell lines confirmed the reported positive relationship between DCAF15 mRNA expression levels and indisulam sensitivity [49] (Figure 6 – figure supplement 1A; R^2=0.33, P=0.02).

We empirically determined that 100nM indisulam treatment moderately lowered RBM39 levels while minimally affecting cell viability and proliferation over a four-day period (Figure 6C-D and [50]). Remarkably, this treatment regime was able to recapitulate the increased CD80 expression seen in K562 DCAF15 KO cells (Figure 6E; 2.14-fold increase), and more modestly, the effects on MHC-I and CD40 expression (1.36-fold and 1.27-fold increase, respectively). CD80 upregulation was first detected 24hrs after treatment initiation and plateaued after 48hrs (Figure 6 – figure supplement 1B). Importantly, indisulam treatment did not further upregulate CD80 in K562 DCAF15 KO cells, suggesting that the pharmaco-modulation of CD80 levels was entirely mediated through DCAF15 (Figure 6F).

To extend these observations to other cell lines, a panel of hematological cancer cell lines was screened to identify those with detectable CD80 expression (Figure 6 – figure supplement 1C). The CML cell line KU812 expressed similar levels of CD80 as K562, whereas the Daudi lymphoma cell line expressed significantly higher basal CD80 levels. These cells lines were subjected to similar 4-day low-dose regimes of indisulam, which only modestly affected the growth and viability of the cells (Figure 6 – figure supplement 1D). Both Daudi and KU812 cells up-regulated CD80 levels after indisulam treatment (Figure 6G; 2.45-fold for Daudi, 1.71-fold for KU812). Indisulam was not able to induce *de novo* CD80 expression in CD80-negative cell lines (Figure 6 – figure supplement 1E). Thus, in certain cellular contexts, aryl sulfonamides are immuno-modulatory agents that alter co-stimulatory protein levels by disrupting the normal functions of DCAF15.

Reduced DCAF15 expression is associated with improved survival in AML patients

Given the *in vitro* findings, we hypothesized that lower DCAF15 expression in myeloid malignancies could be associated with better clinical outcomes. We tested this hypothesis using

publicly available acute myeloid leukemia (AML) datasets [54,55]. In both adult and pediatric AML, lower expression of DCAF15 mRNA was associated with increased median overall survival time (Figure 6H-I). The improved survival of DCAF15-low patients was not driven by a correlation between DCAF15 expression and more aggressive AML subtypes (Figure 6 – figure supplement 1F-G). Taken together, these findings indicate that lower DCAF15 function, achieved pharmacologically or by genetic means, is associated with favorable immunophenotypes *in vitro* and improved outcomes in AML patients.

Cohesin complex members are CRL4-DCAF15 E3 ligase client proteins

The normal substrate repertoire of DCAF15 is unknown. To systemically identify direct DCAF15 client proteins, we undertook proximity-based proteomic analysis of DCAF15 interaction partners (Figure 7A). DCAF15 was fused to a promiscuous bacterial biotin ligase [56] ("DCAF15-BioID") and stably expressed in K562 cells, enabling recovery of interaction partners by streptavidin pull-down. We first confirmed that exogenous C-terminally tagged DCAF15 was able to rescue DCAF15 KO phenotypes and associate with CRL4 complex members DDB1 and CUL4A (Figure 5 – figure supplement 1B-D and Figure 7 – figure supplement 1A). During stable DCAF15 overexpression, we observed that the basal concentration of biotin in the media (~3μM) was sufficient to induce BioID activity in the absence of exogenous (50μM) biotin supplementation (Figure 7B). However, proteasome inhibition by MG132 increased accumulation of DCAF15-BioID and biotinylated species. As a control, results were compared to a GFP-BioID fusion, expected to generically biotinylate proteins. GFP-BioID accumulated much more readily than DCAF15-BioID, and its biotinylation activity was not affected by MG132 treatment.

After 24hrs of biotin and MG132 treatment, biotinylated protein species were recovered under stringent denaturing conditions. Isobaric labeling and mass spectrometry were used to quantitatively compare the DCAF15 interactome to the GFP interactome (Figure 7C and Table S5). This approach clearly recovered DCAF15 and the core CRL4 complex, including DDA1, DDB1 and CUL4A (DCAF15: 155.6-fold change, P=2.5e-152; DDA1: 24.5-fold change, P=6.5e-139; DDB1: 4.86-fold change, P=8.1e-21; CUL4A: 3.8-fold change, P=8.5e-18).

Surprisingly, two of the most differentially biotinylated proteins were the cohesin complex members SMC1A and SMC3 (SMC1: 2.39-fold change, P=0.00098; SMC3: 2.76-fold change, P=5e-5). We confirmed the interaction between DCAF15-BioID and endogenous SMC1 and 3 by streptavidin-pulldown followed by western blotting (Figure 7D). To determine whether this association with cohesin was a generic feature of CRL4 complexes or specific to the CRL4 loaded with DCAF15, we examined the interaction partners of a different substrate adaptor. DCAF16 is a nuclear-localized CUL4 substrate adaptor, which, like DCAF15, interacts with DDB1 despite lacking a canonical WD40 docking domain [32]. When stably expressed in K562 cells, DCAF16-BioID fusions accumulated similarly to DCAF15-BioID, interacted with DDB1 but did not biotinylate SMC proteins (Figure 7E). As low concentrations of indisulam phenocopy certain aspects of DCAF15 depletion (Figure 6), we asked whether indisulam treatment would alter the interaction of DCAF15 with cohesin. DCAF15-BioID cells were pre-treated with indisulam for 72hrs prior to biotin and MG132 addition. This treatment regime lead to substantial indisulam-dependent biotinylation of RBM39 and reduced recovery of biotinylated SMC proteins (Figure 7E).

To test whether DCAF15 promoted SMC1 ubiquitination, we co-transfected 293T cells with his-tagged ubiquitin, DCAF15 and SMC1A, and purified ubiquitinated species under denaturing conditions by nickel affinity chromatography. Co-expression of DCAF15, but not GFP, led to the recovery of poly-ubiquitinated SMC1A (Figure 7F). Treatment with indisulam reduced the amount of ubiquitinated SMC1A recovered. These orthogonal proteomic and biochemical assays support the notion that cohesin proteins are *bona fide* client ubiquitination substrates for DCAF15, with these interactions impaired by DCAF15-engaging aryl sulfonamide drugs.

Discussion

Clinical and experimental data have revealed that disrupting optimal antigen presentation levels is a common mechanism by which cancer cells escape recognition by the adaptive immune system. We performed CRISPR-Cas9 screens using NK-92:K562 co-cultures to uncover perturbations that enhance natural killer mediated anti-cancer immunity. We discovered and characterized how disruption of DCAF15 or PTPN2 sensitizes a variety of cancer cell types to both NK-92 and

426 primary NK cells. In addition, the screens clearly identified known lymphocyte adhesion factors
427 and aNKR/iNKR ligands, such as ICAM1, NCR3LG1, CD58, CD84 and NECTIN2. Performing
428 additional genetic screens on diverse cancer cell lines and natural killer subtypes will enable a
429 more complete understanding of the relative importance of various aNKRs and iNKRs and should
430 identify novel immunotherapeutic targets.
431
432 There was a strong IFNγ signature within our NK-92:K562 screens. We determined that disruption
433 of PTPN2, a negative regulator of IFNγ signaling, consistently enhanced NK cell sensitivity.
434 Interestingly, preventing cancer cell IFNγ signaling had a much more variable effect than removing
435 negative feedback on the pathway, promoting resistance or sensitization to NK cells in target and
436 effector cell dependent manner. This variability likely reflects the complexity of cancer cell IFNγ
437 signaling, which can include MHC upregulation, growth suppression and immunomodulation.
438
439 In K562 cells, PTPN2 KO rendered IFNγ treatment growth suppressive, likely through the
440 induction of apoptosis, while also enhancing the immunomodulatory effects of the cytokine. The
441 immunophenotypic changes include enhanced MHC-I expression, which likely inhibits full
442 activation of NK cell cytotoxicity, especially in primary NK cells that express a broader KIR
443 repertoire than NK-92 cells [22]. PTPN2 disruption has previously been shown to enhance activated
444 T-cell mediated killing, as well as potentiate the effect of immunotherapy in syngeneic tumor
445 models [9,10,57]. These data suggest that targeting PTPN2 may be a generalizable strategy to sensitize
446 tumor cells to multiple arms of the immune system.
447
448 The importance of the cancer cell IFNγ response prompted us to systemically identify
449 perturbations that modulated IFNγ signaling, as read out by cytokine-induced MHC-I
450 upregulation. As expected, this screen clearly delineated the proximal components of the IFNγ-
451 JAK-STAT pathway, as well as the antigen processing/presentation machinery. Surprisingly,
452 disruption of DCAF15, a poorly characterized substrate adaptor for the CRL4 E3 ligase, was a top
453 scoring hit in both the MHC-I and NK screens. We therefore focused our efforts on understanding
454 the role of DCAF15 in this context. We determined that DCAF15 KO cells did not have a grossly
455 dysregulated response to IFNγ, but scored in the MHC-I screen due to higher unstimulated levels
456 of MHC-I. This change reflected a broader phenotypic switch in DCAF15 KO cells reminiscent

of APC activation, including the upregulation of a variety of co-stimulatory and antigen-presenting molecules (Figure 7G). Higher CD80 levels in DCAF15 KO cells were especially important for increasing NK-92 cell triggering. Cross-talk between APCs and NK cells is a well-established phenomenon that mutually regulates both cell types [58]. These interactions, which often occur at sites of inflammation or secondary lymphoid organs, can promote APC maturation or lysis in a context-dependent fashion. Further work is needed to determine whether DCAF15 plays a role in the activation of APCs and their interactions with NK cells.

Our data suggest that the surface factors upregulated by DCAF15 disruption are not direct client proteins of the substrate receptor, but rather represent events secondary to altered turnover of the normal DCAF15 client protein(s). We pioneered a novel approach to systemically purify substrates of DCAF family members, as conventional biochemical methods are poorly suited to recover the transient, low-affinity interactions between substrate adaptors and client proteins. The use of DCAF-BioID fusion proteins and proteasome inhibition protects labile substrates from degradation and robustly recovers biotinylated proteins under stringent, denaturing conditions. We anticipate this will be a generalizable strategy for discovering client proteins for the whole family of CUL4 CRL substrate receptors.

Proteomic analysis and subsequent validation experiments showed that DCAF15 loaded into CLR4 complexes, interacted with cohesin complex members SMC1 and SMC3, and promoted their ubiquitination. We were intrigued by these interactions given the similar CRISPR screening scoring pattern of DCAF15 to the cohesin factors STAG2 and HDAC8 (Figure 2E); the shared roles of cohesin and CRL4 E3 ligases in DNA metabolism, organization, replication and repair [34,59,60]; and the ability of cohesin mutations to dysregulate hematopoietic differentiation in myeloid malignancies [35]. Rather than globally controlling SMC protein levels, we speculate that CRL4-DCAF15 complexes ubiquitinate cohesin at specific genomic sites to regulate chromatin topology or repair (Figure 7G). In this model, disruption of either STAG2, HDAC8 or DCAF15 impair cohesin function with overlapping phenotypic consequences. Further work is needed to elaborate the control of cohesin function by DCAF15 and how this may promote APC-like differentiation.

Recently, it was discovered that aryl sulfonamide drugs including indisulam are capable of binding to DCAF15 and altering CRL-DCAF15 substrate specificity towards the splicing factor RBM39 [49,50]. The cytotoxic effects of indisulam were driven by splicing defects resulting from RBM39 degradation. Our studies confirmed indisulam-induced RBM39 degradation and the indisulam-dependent interaction between DCAF15 and RBM39. We also discovered indisulam-induced phenotypes attributable to inhibition of DCAF15's normal functions. Concentrations of indisulam with limited RBM39 degradation or cytotoxicity had immunomodulatory properties that phenocopied genetic DCAF15 disruption. Biochemically, the recruitment of endogenous client proteins to CRL4-DCAF15 and subsequent ubiquitination was impaired by indisulam treatment. We also determined that AML patients with naturally occurring lower levels of DCAF15 had improved overall survival. While these clinical data are preliminary in nature, they provide a rationale for drugging DCAF15 in myeloid neoplasms, achieved through judicious dosing of existing anti-cancer sulfonamides or the development of pure DCAF15 inhibitors.

FIGURES

Figure 1. A genome-scale CRISPR screen identifies modulators of NK effector functions

A) Overview of the genome-scale NK CRISPR screening system.

B) K562 population doublings (PDs) during the CRISPR screen, as measured by total number of live cells. Note that early timepoints from the co-culture reflect the presence of both K562 and NK-92 cells.

C) Analysis of the NK CRISPR screen results. Changes in sgRNA abundance were compared between the 2.5:1 E:T co-culture condition and day 15 dropout cells using the MAGeCK algorithm. The top 10 enriched or depleted genes are shown, as rank-ordered by MAGeCK score; other manually selected genes are highlighted with their rank indicated. FDR, false discovery rate.

D) Overview of high-scoring components of the tumor-immune synapse and IFNγ signaling pathway recovered by the screen. sgRNAs against genes enriched after exposure to NK-92 cells are marked in red, while depleted sgRNAs are marked in blue.

Figure 1 – figure supplement 1. Optimization of NK CRISPR screens.

A) Western blot showing spCas9 expression in clonal isolates of K562 cells infected with a Cas9-expressing lentivirus. Asterisk highlights the clone used for screening purposes.

B) Measurement of Cas9 activity using an EGFP disruption assay. Cas9-expressing K562 cells were infected at a low MOI with a lentivirus expressing EGFP and a sgRNA targeting EGFP. The percent of cells that lost EGFP expression was measured over time by flow cytometry.

C) Measurement of Cas9 activity using sgRNAs targeting mismatch-repair (MMR) complex members. A Cas9-expressing K562 clonal isolate was infected at a low MOI with a lentivirus expressing sgRNAs against core members of the MMR complex. Protein disruption was measured by western blot 10 days after sgRNA infection. Note that certain MMR complex members depend on other binding partners for stability.

D) Experimental design for determining selective pressure of different E:T cell ratios. K562 cells were labeled with carboxyfluorescein succinimidyl ester (CFSE) prior to co-culture with NK-92 cells.

E) Effect of increasing E:T cell ratio on total number of viable target cells over time. During early timepoints, CFSE fluorescence was used to generate target cell counts. At later timepoints, total cell counts accurately reflected target cell counts due to NK-92 cell death.

F) Representative image of NK-92:K562 co-cultures at 5:1 E:T ratio. NK-92 cells (unlabeled) form aggregate structures enveloping the target cells (green). Scale bar, 250μM.

Figure 1 – figure supplement 2. Additional NK CRISPR screen data.

A) Analysis of the NK CRISPR screen results performed at a lower E:T ratio. sgRNA abundance was compared between the 1:1 E:T ratio co-culture condition and day 15 dropout cells using the MAGeCK algorithm. The computed false discovery rate (FDR) is plotted against the -log10 transformation of the MAGeCK score. The top 5 enriched or depleted genes are shown, as rank-ordered by MAGeCK score; other manually selected genes are highlighted with their rank indicated in parentheses.

Supplemental Table 1. Design of genome-scale CRISPR library. sgRNA sequences and coordinates of the intended target locus are provided.

Supplemental Table 2. NK CRISPR screen data. Normalized sgRNA counts and MAGeCK analysis output are provided.

Figure 2. A phenotypic screen based on MHC-I upregulation to identify modulators of the IFNγ response

A) Flow cytometry measurement of MHC-I expression in K562 cells transduced with the indicated sgRNAs after 24hrs of 10ng/ml IFNγ treatment.

B) Fold upregulation of MHC-I expression after IFNγ treatment in K562 cells transduced with the indicated sgRNAs. Mean and standard deviation are shown. *** P value= 0.0002, ** P value=0.03, Mann-Whitney test.

C) Design of CRISPR screen for IFNγ-induced upregulation of MHC-I expression. SSC, side-scatter.

D) Analysis of the MHC-I upregulation CRISPR screen results. The MAGeCK algorithm was used to compare sgRNA abundance between cells in the bottom two and top two deciles

of MHC-I expression. The false discovery rate (FDR) is plotted against the -log10 transformation of the MAGeCK score. The top 5 to 10 enriched or depleted genes are shown, as rank-ordered by MAGeCK score; other manually selected genes are highlighted with their rank indicated in parentheses.

E-F) Comparison of the NK and MHC screening results. Results of each screen were rank-ordered based on their MAGeCK score. Select genes are highlighted.

Figure 2 – figure supplement 1. Confirmation of gene disruption in K562 cells.

A) Western blot of total STAT1 levels in K562 cells infected with control or STAT1 sgRNAs.

B) Western blot of PTPN2 levels in K562 cells infected with control or PTPN2 sgRNAs.

Supplemental Table 3. Raw MHC-I screen data. Normalized protospacer counts and MAGeCK analysis output are included.

Figure 3. Disruption of DCAF15 enhances NK effector functions

A) Experimental design of competitive co-culture experiments, with FACS data illustrating a hypothetical sgRNA that enhances NK-mediated target cell clearance.

B) Representative results from NK-92:K562 competitive co-culture experiments performed at a 2.5:1 E:T ratio.

C) Results of competitive co-culture performed at a 2.5:1 E:T ratio and measured 48-96hrs after challenge of K562 cells with NK-92 cells. Mean and standard deviation are shown. *** P-value <0.0001, Mann-Whitney test.

D) Results of competitive co-culture performed at a 1:1 E:T ratio and measured 48-96hrs after challenge of K562 cells with IL-2 activated isolated peripheral NK cells. ** P-value <0.01, * P-value =0.06, Wilcoxon matched-pairs signed rank test.

E) Results of competitive co-culture performed at a 2.5:1 E:T ratio and measured 48-96hrs after challenge of Daudi cells with NK-92 cells. Mean and standard deviation are shown. *** P-value <0.0001, ** P-value=0.0022, * P-value=0.09, Mann-Whitney test.

F) Flow cytometry analysis of NK cell degranulation (cell surface CD107A expression) after 2hr coculture of primary NK cells with indicated target cell types at 2.5:1 E:T ratio. Line

593 indicates median value. ** P-value =0.095, * P-value=0.067, NS P-value>0.10, Mann-
594 Whitney test.
595
596 **Figure 3 – figure supplement 1. Confirmation of gene disruption in K562 and Daudi cells.**
597 A) Measurement of cell surface NECTIN2 expression by flow cytometry in K562 cells
598 expressing control or NECTIN2 sgRNAs. Gates show background levels of fluorescence.
599 B) Measurement of cell surface ICAM1 expression by flow cytometry in K562 cells
600 expressing control or ICAM1 sgRNAs. Gates show background levels of fluorescence.
601 C) Measurement of DCAF15 mRNA expression by RNAseq in K562 cells transduced with
602 control or DCAF15 sgRNAs.
603 D) Western blot of PTPN2 levels in Daudi cells infected with control or PTPN2 sgRNAs.
604 E) Measurement of cell surface ICAM1 expression by flow cytometry in Daudi cells
605 expressing control or ICAM1 sgRNAs. Gates show background levels of fluorescence.
606 F) Measurement of DCAF15 mRNA expression by RNAseq in Daudi cells transduced with
607 control or DCAF15 sgRNAs.
608
609 **Figure 3 – figure supplement 2. Co-culture of primary NK cells with K562 cells.**
610 A) Flow cytometry analysis of purity of isolated peripheral NK cells 24hrs after IL-2
611 stimulation.
612 B) Flow cytometry analysis of activation status of CD3-CD56+ NK cells after 24hrs of IL-2
613 stimulation.
614
615 **Figure 4. DCAF15 disruption leads to an inflamed state distinct from dysregulated IFNγ-**
616 **JAK-STAT signaling**
617 A) Flow cytometry measurement of cell surface MHC-I expression in K562 cells transduced
618 with the indicated sgRNAs after 24hrs of 10ng/ml IFNγ treatment. *** P <0.0001; ** P=
619 0.0044, Mann-Whitney test.
620 B) Western blots illustrating total and phosphorylated STAT1 after 30 minutes of 1ng/ml IFNγ
621 treatment in K562 cells infected with the indicated sgRNAs.

C) Growth rate of K562 cells expressing the indicated sgRNAs, cultured under basal conditions ("untreated"), treated 24hrs with 10ng/ml IFNγ ("IFNγ pulse"), or continuously retreated with 10ng/ml IFNγ every day ("IFNγ constant").

D) Principle component analysis (for principle components (PC) 1 and 3) of transcriptomes from K562 cells expressing the indicated sgRNAs and treated +/- 10ng/ml IFNγ for 24hrs.

E) Selected GO terms, identified by RNA-seq, enriched in DCAF15 KO cells. Negative log10 transformation of the Benjamini-Hochberg corrected P value.

F) Volcano plot of genes differentially expressed between DCAF15 KO cells compared to control KO cells. Selected genes are highlighted. The FDR-corrected P-value generated from a likelihood ratio test (Q-value) is plotted against an approximate measure of the fold change in expression (Beta value).

Figure 4 – figure supplement 1

A) Growth rate of K562 cells expressing sgRNAs against DCAF15 or a control gene. Results from 2-3 independent experiments and 2-3 different sgRNAs per gene. Mean and standard deviation are shown. DCAF15 sgRNAs, 1.1+/-0.01 population doublings per day. Control sgRNAs, 1.13+/-0.03 population doublings per day.

B) Volcano plot of genes differentially expressed in control K562 cells after 24hrs of IFNγ treatment. Selected genes are highlighted. Genes that were off-scale and could not be plotted are shown in the oval. The FDR-corrected P-value generated from a likelihood ratio test (Q-value) is plotted against an approximate measure of the fold change in expression (Beta value).

C) Flow cytometry analysis of the change in cell surface expression of the indicated cell surface markers in K562 cells transduced with the indicated sgRNAs after 24hrs of 10ng/ml IFNγ treatment. ** P value= 0.003, * P value=0.026, Mann-Whitney test.

D) Gene set enrichment analysis (GSEA) of genes differentially upregulated in PTPN2 KO cells. nES, normalized enrichment score. Categories with a FDR Q-value of <0.1 are shaded in blue.

E) GSEA of genes differentially upregulated in PTPN2 KO cells after IFNγ treatment.

Supplemental Table 4. List of differentially expressed genes determined by RNA-seq of control, DCAF15 or PTPN2 KO K562 cells.

Figure 5. DCAF15 knockout cells enhance NK-92 triggering via CD80 expression

A) Flow cytometry measurements of the indicated cell surface markers in K562 cells expressing the indicated sgRNAs. N=9-24 samples per condition. *** P<0.0001, ** P=0.001, ns P>0.1, Mann-Whitney Test.

B) Flow cytometry measurement of CD80 surface expression in control K562 cells or those transduced with lentivirus to overexpress CD80. Gate shows level of background fluorescence in unstained cells.

C) Results of competitive co-culture between indicated K562 cell types and NK-92 cells, performed at 1:1 E:T ratio. K562 cells were unmanipulated ("control") or overexpressed wild-type CD80 ($CD80^{wt}$) or mutant CD80 ($CD80^{mut}$; contains Q65A and M72A point mutations that abrogate CD28 binding). * P=0.005, ** P=0.0007, NS P>0.1, unpaired T test.

D) Experimental design of CD80 blockade experiment.

E) Effect of blocking antibodies to CD80 on NK-92 activation, measured by CD107 flow cytometry on NK-92 cells after 4hrs of co-culture. Data points from experiments performed on the same day are joined by lines of the same color. ** P=0.03, * P=0.06, ns P>0.1, Wilcoxon matched-pairs signed rank test. Experiment performed 4 times, 2x sgRNAs per condition.

F) Percent decrease in NK-92 degranulation after CD80 antibody treatment of indicated target cells. Data points from experiments performed same day are joined by lines. Mean is indicated. ** P=0.03, Wilcoxon matched-pairs signed rank test.

Figure 5 – figure supplement 1

A) Flow cytometry measurements of the indicated cell surface markers in K562 cells expressing the indicated sgRNAs. N=2-14 samples per condition. Ns P>0.1, * P=0.04, ** P=0.01, Mann-Whitney Test.

B) Experimental design for rescuing DCAF15 disruption in K562 by lentiviral expression of a sgRNA-resistant DCAF15 open reading frame.

C) Western blot of DCAF15 rescue construct expression.

D) Flow cytometry measurements of the indicated cell surface markers in K562 cells expressing the indicated sgRNAs and rescue constructs. N=6-24 samples per condition. *** P<0.0001, ** P=0.004, Mann-Whitney test.

E) Flow cytometry measurement of CTLA4 and CD28 expression on NK-92 cells. Gates show background fluorescence levels in unstained cells.

F) Flow cytometry measurement of CD28 expression in peripheral unstimulated NK cells.

Figure 6. The anti-leukemia drug indisulam inhibits DCAF15 function

A) Proposed model for DCAF15 gain- and loss-of-function phenotypes triggered by indisulam treatment.

B) Dose response of K562 cells expressing the indicated sgRNAs to indisulam. Relative viability measured by ATP content. N=2 experiments. Mean and standard deviation are shown.

C) Growth of K562 cells treated with 0.1μM indisulam over 4 days. N=12 per timepoint. Mean and standard deviation are shown.

D) Western blot for total RBM39 levels in K562 cells after 0.1μM indisulam treatment for the indicated number of days.

E) Flow cytometry measurements of the indicated cell surface markers in K562 cells after indisulam treatment. Mean and standard deviation are shown. *** P<0.0001, ** P=0.0085, * P=0.013, mean significantly different from 1, one sample T test.

F) CD80 expression measured by flow cytometry in indisulam-treated K562 cells expressing the indicated sgRNAs. Mean and standard deviation are shown. N=4-6 samples. ** P=0.0095, * P=0.0286, ns P>0.1, Mann-Whitney test.

G) Effect of indisulam treatment on CD80 expression in the indicated cell lines. N=3-12 samples. Mean and standard deviation are shown. *** P<0.0001, ** P= 0.0066, mean significantly different from 1, one sample T test.

H) Kaplan-Meier analysis of overall survival in adult AML patients from TCGA LAML project stratified by DCAF15 expression. “DCAF15 high” and “DCAF15 low” represents patients in top or bottom 50% of DCAF15 expression, respectively. N=142 patients. 95%

confidence interval shown. Median survival, 16.17 vs 12.18 months. P-value from log-rank test.

I) Kaplan-Meier analysis of overall survival in pediatric AML patients from TARGET project stratified by DCAF15 expression. "DCAF15 high" and "DCAF15 low" represents patients in top or bottom 20% of DCAF15 expression, respectively. N=76 patients. 95% confidence interval shown. Median survival, 21.17 vs NA. P-value from log-rank test.

Figure 6 – figure supplement 1

A) Relationship between DCAF15 mRNA expression and indisulam sensitivity across a panel of cell lines.

B) Time-course of CD80 expression after indisulam treatment in K562 cells measured by flow cytometry. Blue shading indicates period of CD80 upregulation. N=2-4 samples per timepoint. Mean and standard deviation are shown.

C) CD80 expression measured by flow cytometry across a panel of cancer cell lines. Dashed line indicates background level of antibody staining, with cell lines in red have expressing above background levels of the protein. CML, chronic myelogenous leukemia. BL, Burkitt's lymphoma. AML, acute myeloid leukemia. AMoL, acute monocytic leukemia. T-ALL, T-acute lymphoblastic leukemia. MM, multiple myeloma. ALCL, anaplastic large cell lymphoma.

D) Growth of Daudi and KU812 cells treated with 0.1μM indisulam over 4 days. N=3 per timepoint. Mean and standard deviation are shown.

E) Fold change in CD80 expression in the indicated cell lines after 4 days treatment with 0.1μM indisulam.

F) Box and whisker plot of DCAF15 expression in TCGA LAML samples, stratified by subtype using the French American British (FAB) AML classification scheme. Analysis from UALCAN portal [61]. Subtypes with significantly different median expression values are indicated.

G) FAB classification of adult AML patients in the TCGA LAML project, stratified by top 50% ("DCAF15 high") or bottom 50% ("DCAF15 low") of DCAF15 expression.

Figure 7. Cohesin complex members are CRL4-DCAF15 E3 ligase client proteins

744

745 A) Experimental system for discovering DCAF15 interaction partners by proximity ligation.

746 B) Indicated constructs were stably expressed in K562 cells, and biotinylated proteins detected
747 by HRP-conjugated streptavidin ("α-biotin"). Asterisks denote major endogenous biotin-
748 containing proteins. "MG132" and "Biotin" refer to 18hrs treatment with 5μM MG132 or
749 50μM biotin.

750 C) Proteins identified by quantitative mass spectrometry as differentially biotinylated by
751 DCAF15-BioID as compared to GFP-BioID. Log2-fold changes are plotted against
752 precision of the measurement (1/ coefficient of variation). Colors denote the posterior
753 probability that a protein fold change was small (referred to as "P-null" in the legend), as
754 explained in the methods. Data points in red are select CRL4 core complex members. Data
755 points in blue are endogenous biotin-containing proteins.

756 D-E) Affinity capture of biotinylated proteins by streptavidin beads ("biotin IP") and detection
757 by western blot. Indicated constructs were stably expressed in K562 cells. "Indisulam"
758 refers to 48hrs 0.1μM indisulam treatment prior to MG132 and biotin addition.

759 F) Capture of 6xhis-ubiquitinated species by nickel chromatography under denaturing
760 conditions and detection by western blot. The indicated expression plasmids were
761 transiently transfected into 293T cells. Input samples were prepared from whole cell lysates
762 (WCL). "MG132" and "Indisulam" refer to 12hrs treatment with 10μM MG132 or 2μM
763 Indisulam prior to harvest.

764 G) Model of DCAF15 function.

765

766 **Figure 7 – figure supplement 1**

767 A) Exogenous DCAF15 interacts with CRL4 core complex members. Indicated constructs
768 were stably expressed in K562 cells. Anti-Flag immunoprecipitations were performed and
769 analyzed by western blot.

770

771 **Supplemental Table 5.** Comparison of biotinylated proteins recovered from K562 cells
772 expressing DCAF15-BIoID or GFP-BioID using isobaric labeling and mass spectrometry.

773

774 **Supplemental Table 6.** List of sgRNA sequences used.

775

776 **Supplemental Table 7.** List of antibodies used.

777

778 **Supplemental Table 8.** Primer design for sequencing sgRNA libraries.

779

Materials and methods

Cell lines

All cell lines were purchased from ATCC and were tested monthly for mycoplasma contamination. Cell lines other than NK-92 were maintained in RPMI supplemented with 10% FBS, 1mM GlutaMAX and 1% antibiotic, antimycotic. NK-92 cells were grown in Myelocult H5100 (Stem cell Technologies) supplemented with 100U/ml human IL-2 (Peprotech cat#200-02). IL-2 stock solution was made by reconstituting lyophilized cytokine to 10e6 U/ml in 50mM acetic acid, 0.1% BSA in PBS.

Construction of the CRISPR Library

CRISPR screening was performed using bespoke genome-scale libraries, to be described in detail elsewhere. In brief, the sgRNA library was designed with 120,021 sgRNAs present, representing 6 guides each against 21,598 genes and 4 guides each against 1,918 miRNAs, as well as 1000 non-targeting negative control guides (Table S1). sgRNAs targeting protein-coding genes were based on the Avana libraries [62]. sgRNAs targeting miRNAs were based on the design of the Gecko v2.0 libraries [63]. The protospacer library was synthesized by Twist Biosciences. The synthesized oligo library was amplified using emulsion PCR followed by purification. The vaccinia virus DNA polymerase was used to clone the protospacers into a lentiviral construct (In-fusion, Takara). The lentiviral construct was linearized by Bfua1 digestion (New England Biolabs). To ensure complete digestion, Bfua1 activity was stimulated by addition of 500nM of a double-stranded oligo containing a Bfua1 site (5' atagcacctgctata 3') (based on [64]).

The guide RNAs were expressed from a human U6 promoter, using a modified sgRNA design (A-U flip, longer stem-loop) previously described [65]. An EF1a-Puro-T2A-cerulean-wpre ORF was used for selection purposes and for measuring infection rates. The library was electroporated into MegaX cells and plated across 37x 500cm^2 LB-carbenicillin plates. The library was recovered and pooled by scraping and column-based plasmid purification (Zymopure GigaPrep).

Preparation of virions

16M 293T cells were plated onto 177cm^2 dishes (9x plates total). 24hrs later, cell media was replaced with 32mls of DMEM+10% FBS (D-10). Cells were transfected with the library by lipofection (per plate: 158ul lipofectamine 2000, 8mls of Optimem, 3.95µg of VSVG, 11.8µg of Pax2, 15.78µg of library). The transfection mixture was left on the cells overnight, then changed to 25mls of D-10. Viral supernatant was collected 48hrs later. Debris was removed by centrifugation at 200g. Aliquots were flash-frozen and stored at -80°C.

Validation of the Cas9-expressing cell line used for screening

K562 cells were lentivirally infected with an EF1a-spCas9-T2A-blastR construct. Following 10µg/ml blasticidin selection, cells were dilution cloned. Clonal isolates with high levels of cas9 expression (as determined by western blot) were selected for further characterization. To determine the kinetics and efficacy of gene cutting under screening conditions (*e.g.*, low multiplicity of infection (MOI)) of the sgRNA construct), cells were infected with a lentiviral construct expressing both EGFP and a sgRNA targeting GFP. Following puromycin selection, the loss of EGFP expression was monitored by flow cytometry. In other experiments, the ability to effectively deplete endogenous proteins was determined by using a series of sgRNAs targeting the mismatch repair complex and measuring protein depletion by western blot.

NK screen

Five hundred million spCas9-expressing K562 cells were mixed with CRISPR sgRNA library virions and 1L of media, then distributed across 34 6-well plates. Cells were spin-infected at 1900 rpm for 30 min at room-temperature with CRISPR library virus, conditions calculated to achieve a MOI of ~0.3 and 1000 cells per sgRNA library representation. MOI was measured by tracking the percent of the population expressing the cerulean marker found in the sgRNA library. Cells were incubated overnight in viral supernatant prior to being pooled, spun down to remove virions, and returned to spinner-flask culture (Bell-Flo Flask, Bellco Glass Inc). 24 to 48hrs post-infection, 2µg/ml puromycin selection was started for four days. Cells were maintained in log-growth phase with a minimal representation of 500M cells. Seven days post guide-infection, NK cell challenge was initiated. For the 2.5:1 E:T challenge, 100M K562 cells were mixed with 250M NK-92 cells in 1L of Myelocult, and split across 25 177cm^2 dishes. For the 1:1 E:T challenge, 100M K562 cells were mixed with 100M NK-92 cells in 400mls of Myelocult, and split across 10 177cm^2 dishes.

As a control, K562 cells were continuously propagated in RPMI media. 2 days after initiating the NK-92 challenge, the co-culture was switched to RPMI media. NK-92 cells, when grown in RPMI without IL-2, are rapidly lost from the culture. Six days after the media switch, 100M cell pellets were generated for library construction. All cell pellets were stored cryopreserved in cell-freezing media (Gibco #12648).

MHC-I screen

Generation of K562 cells expressing the sgRNA library was performed as described above. On day 8 post-guide infection, 150M cells were stimulated with 10ng/ml IFNγ (R&D Systems 285-IF). 24hrs later, cells were spun down, washed, and stained in 3mls of 1:200 anti-HLA ABC-APC (W6/32 clone, BioLegend) in PBS, 2% FBS for 30min at 4°c. Approximately 10M of the brightest 20% and dimmest 20% of cells were sorted (BD FACSAria Fusion). Cell purity was determined to be >95% by re-analysis post-sorting. A replicate of this experiment was performed on day 14 post-guide infection.

CRISPR library preparation and sequencing

Genomic DNA was prepared by thawing cryopreserved cell pellets and proceeding with DNA extraction using column-based purification methods (NucleoSpin Blood XL, Machery-Nagel). Protospacer libraries were generated by a two-step PCR strategy, modified from [66]. In the first round of PCR, 150µg of gDNA (equivalent to 15M K562 cells and 125-fold coverage of the library) was used in a 7.5ml PCR reaction to amplify the protospacers. This reaction was performed using a 500nM mixture of primers containing 0-9bp staggers, to ensure base-pair diversity during Illumina sequencing (see supplemental table S7). The reaction was performed with Phusion master mix (New England Biolabs) and 3% DMSO with the following cycling conditions: 1 cycle X 30 s at 98°C, 21 cycles X 15 s at 98°C, 20 s at 63°C, 15 s at 72°C, 1 cycle X 2 min at 72°C. In the second round of PCR, 4µl of the initial PCR product was used as the template in a 200µl PCR reaction to make the sample compatible with Illumina chemistry and to add unique I5 and I7 barcodes to the sample. The reaction was performed with Phusion master mix (New England Biolabs), 500nM primers and 3% DMSO with the following cycling conditions: 1 cycle X 30 sec at 98°C, 12 cycles X 15 s 98°C, 20 s at 60°C, 15 s at 72°C, 1 cycle X 2 min at 72°C. The library was size-selected first by a 1:1 SPRI bead selection (AMPure XP beads, Beckman Coulter),

quantified by high-sensitivity dsDNA Qubit (ThermoFisher Scientific), and pooled. An agarose size selection step (PippinHT, Sage Science) was performed prior to sequencing on an Illumina Hiseq4000.

Screen analysis

Libraries were sequenced to a depth of ~20 million reads per condition. Reads were aligned to the sgRNA library using bowtie2. Protospacer count tables were generated from these alignments with python scripts and processed with MAGeCK. MAGeCK analysis was used to score and prioritize sgRNAs, using default settings in the algorithm [23]. A subset of genes, mostly from highly related gene families, have more than 6 sgRNAs targeting them. As the MAGeCK scoring method tends to prioritize consistency of effect over magnitude of effect, genes with more than 6 guides targeting them were excluded from the analysis. MAGeCK scores were -log10 normalized, and values were plotted against FDR values.

NK-92 competitive co-culture assay

Cas9-expressing K562 or Daudi cells were transduced at a high MOI with a lentiviral sgRNA construct expressing the guide of interest, puromycin resistance and CMV promoter-driven expression of either a red or green fluorescent protein. Knockout cell populations were maintained in a polyclonal state. Gene disruption was confirmed at the protein level by flow cytometry or western blot, and by RNA-seq when antibody reagents were not available. Complete knockout in >90% of the population was routinely achieved (Figure 2 – figure supplement 1 and Figure 3-figure supplement 1). Cells were counted and 0.25M red-labeled test cells were mixed with 0.25M green-labeled control cells (expressing a sgRNA against an olfactory receptor gene). The mixture was either grown in RPMI or mixed with 1.25M NK-92 cells in 4mls Myelocult media in 6-well plates. The ratio of green-to-red cells was measured 2 to 4 days post-challenge, with the fold-change normalized to the ratio in the non-challenged state (to control for differences in basal cell growth rate).

Primary NK cell isolation

PBMCs were isolated from leukocyte-enriched blood of human donors (Stanford Blood Center). Donors were not genotyped or pre-screened for infectious disease markers. Natural killer cells

were isolated by negative selection using magnetic columns (Miltenyi 130-092-657). Purity post-selection was routinely >97% CD56+ CD3-. Isolated NK cells were plated at 1M/ml density in 96-well u-bottom plates and stimulated overnight with 1000U/ml IL-2 in complete RPMI with 10% FBS.

Primary NK cell degranulation assay

Following IL-2 activation, NK cells were counted and mixed with target cells in 96-well u-bottom plates. 100,000 NK cells were mixed with 40,000 target cells in a final volume of 200µl for a 2.5:1 E:T ratio. Cells were co-cultured at 37°C for 2 hrs, then stained with anti-CD56-BV421 (1:200) and anti-CD107a-APC (1:200 dilution) for 30m at 4°C. CD107a expression was assayed by flow cytometry in the 7-AAD- CD56+ RFP- GFP- cell population. Primary NK cells exhibited very little basal degranulation in the absence of target cells (<1% CD107a+). The assay was repeated with 6 primary donors with technical duplicates.

Primary NK cell competitive co-culture assay

Following IL-2 activation, NK cells were counted and mixed at a 1:1 E:T ratio with RFP-labeled target cells and GFP-labeled control cells in a 96-well u-bottom plate. 50,000 NK cells were combined with 25,000 Red and 25,000 Green cells in a final volume of 200µl and continuously expanded in 96-well plates to as needed. The ratio of GFP+ to RFP+ cells was measured by flow cytometry on days 2 and 4 post-challenge, and the fold change was normalized to the ratio in the non-challenged state (to control for differences in basal cell growth rate). The assay was repeated with 6 primary donors with technical duplicates.

Flow cytometry

0.5 to 1M cells were spun down and stained with APC-conjugated antibodies for 30mins at 4°c in PBS with 2% FBS. Cells were analyzed on a BD LSRFortessa. The geometric mean fluorescence intensity of singlet, DAPI-excluding cells was measured, and normalized to the background fluorescence of that particular genotype of cells.

DCAF15 rescue experiments

The DCAF15 open reading frame was synthesized based off reference sequence NM_138353, but with silent mutations designed to confer resistance to all three sgRNAs. To ensure resistance to sgRNA-directed gene cutting, silent mutations were introduced to the PAM domain and the proximal region of the protospacer (guide #1: 5' GCTGCACACCAAGTACCAGGTGG to GCTGCACACCAAaTAtCAaGTaG. Guide #2: 5' TGACATCTACGTCAGCACCGTGG to TGACATCTACGTCtcCACaGTaG; Guide #3: 3' GCAGCTTCCGGAAGAGGCGAGGG to GCAGCTTCCGGAAtaaaCGtGGt).

The rescue construct was expressed lentivirally from an EF1a promoter, with a c-terminal 3-flag epitope tag. Rescue cells were selected with hygromycin. The rescue construct was introduced two weeks after the initial introduction of the DCAF15 sgRNAs, and stable cell lines generated by a week of selection in 375μg/ml hygromycin. Expression of the construct was confirmed by lysing cells in PBS+0.1% NP40 (as per [49]) and western blotting for the Flag tag.

CD80 blocking experiments

RFP-labeled target cells (0, 0.75M, or 2.5M) were resuspended in 0.5mls Myelocult + 5μg/ml control (MOPC-21 clone) or blocking CD80 (2D10 clone) antibodies. Cells were incubated for 30 mins at room temperature. 0.5M NK-92 cells in 0.5mls Myelocult were added to the well with 1:200 anti-CD107a-APC antibody. Cells were co-cultured for 4hrs at 37°C. Flow cytometry was used to measure CD107A-APC expression in the NK-92 (RFP-negative) population. NK-92 cells were found to display a basal level of CD107a expression in the absence of effector cells. Increases above basal staining levels were used to define NK-92 degranulation. The experiment was repeated 4 times to establish biological replicates.

CD80 over-expression experiments

A full-length CD80 open reading frame, based on reference sequence NM_005191.4, was synthesized with a c-terminal 3x Flag tag and expressed lentivirally from the EF1a promoter. Over-expressing cells were selected with hygromycin. As a control construct, a mutant version of CD80 was synthesized with Q65A and M72A mutations in the "V-type" Ig-like domain. Each of these residues makes contacts with CTLA4 in published CD80-CTLA4 co-crystal structures [67] and

alanine scanning experiments have shown that these residues are required for CD80 binding to CD28 or CTLA4 [47].

sgRNA sequences used

See supplemental table 6.

Antibodies used

See supplemental table 8.

Cell viability after in vitro cytokine stimulation

Cells were plated at 0.25M/ml in media with or without 10ng/ml IFNγ. Every day, an aliquot of cells was counted (Vi-CELL XR, Beckman Coulter), and cells were diluted in fresh media to maintain them in logarithmic growth phase. Continuously-treated cells were re-fed with fresh 10ng/ml IFNγ every day, whereas pulse-treated cells only received 24hrs of cytokine treatment.

Western Blotting

Cells were counted, spun down and washed in PBS prior to lysis in NP40 lysis buffer (25mM HEPES pH 7.5, 150mM NaCl, 1.5mM $MgCl_2$, 0.5% NP40, 10% glycerol, 2mM DTT) with protease and phosphatase inhibitors. Lysates were normalized by cell count and/or protein concentration. 20-40μg of lysates were used for western blot analysis using standard procedures. Antibody binding was detected by enhanced chemiluminescence (SuperSignal Dura, Thermo Scientific).

RNA-sequencing analysis

Cells were seeded at 0.33M/ml density. Twenty-four hours later, 2M cells were collected. RNA was first purified by TRizol extraction and then further purified using column-based methods and polyA selection. RNAseq libraries were constructed using TruSeq Stranded mRNA Library Prep Kits (Illumina) and were sequenced on an Illumina Hiseq4000 machine using 150bp paired-end reads. Transcript abundances were quantified using Salmon (v0.9.1) in pseudo-alignment mode, without adapter trimming, using the Ensembl GRCh38 transcriptome [68]. Differential expression analysis was performed using Sleuth (v0.29.0) [69]. RNA-seq analysis was executed and visualized

using an in-house web-based platform. RNA sequencing data is available under accession number GEO:GSE134173.

Indisulam treatment

Indisulam (Sigma SML1225) was reconstituted at 10mM in DMSO and stored in single use aliquots at -80°C. For indisulam dose-response experiments, 5000 cells were plated in 384-well plates (Greiner) and treated with indisulam over a 72hr period. A 12-point dose-response was performed between 10μM and 4.9μM of drug, as dispensed by a Tecan D300e. Cell viability was measured by ATP quantification (Cell Titer Glo, Promega). Dose-response measurements were fitted to a sigmoidal curve and an IC50 determined (Prism, GraphPad Software). DCAF15 expression data from different cell lines was downloaded from the Cancer Cell Line Encyclopedia [70] (https://portals.broadinstitute.org/ccle)

For low-dose indisulam experiments, cells were plated at 0.4M/ml in media with or without 100nM indisulam (1:100,000 dilution of stock). Cells were diluted every day in fresh media and drug to maintain them in logarithmic growth phase. Cells were analyzed for CD80 expression 96hrs after initiation of treatment.

AML survival analysis

FPKM RNAseq quantification for patient samples from the TARGET and TCGA LAML cohorts was obtained from the NIH NCI Genomic Data Commons DATA portal (https://portal.gdc.cancer.gov/). Clinical data for that TARGET AML and TCGA LAML cohorts were obtained from the Genomic Data Commons DATA portal and the Broad Institute TCGA Genome Data Analysis Center (http://gdac.broadinstitute.org/) respectively. Patients with matching clinical and transcript abundance data patients were stratified by DCAF15 expression as indicated. Survival time and vital status were defined as 'Overall Survival Time in Days' and 'Vital Status' respectively for the Target AML cohort. For the TCGA LAML study survival time for deceased patients ('patient.vital_status'=dead) was defined as 'patient.days_to_death' while for living patients ('patient.vital_status'=alive) 'patient.days_to_last_followup' was used for survival time. Survival analysis and Kaplan–Meier plots were generated using lifelines software for python (https://doi.org/10.5281/zenodo.2584900).

DCAF15 proximity ligation

K562 cells were infected with lentivirus expressing DCAF15-3flag-BioID-HA-T2A-BlastR, DCAF16-3flag-BioID-HA-T2A-BlastR, or 3flag-GFP-T2A-BioID-HA-T2A-BlastR. Stable cell lines were generated by 10μg/ml blasticidin selection. In triplicate, 20M cells were grown in media supplemented with 50μm biotin and 5μm MG132. 18hrs later, cell pellets were washed three times with ice cold PBS and lysed in mild lysis buffer (PBS 0.1% NP40 + PI/PPI), conditions determined to maximize the solubility of over-expressed DCAF15. 1mg of clarified lysate was used for enrichment of biotinylated species. Lysates were mixed with 60ul of streptavidin beads (Pierce #88817) for 4hrs at 4°c in 500μl total volume. Beads were collected on a magnetic column, washed twice with 1ml RIPA buffer (25mM HEPES-KOH pH 7.4, 150mM NaCl, 1% Triton X-100, 0.5% sodium deoxycholate, 0.1% SDS, 1mM EDTA) and three times with 1ml urea buffer (2M urea, 10mM TRIS-HCl pH 8.0).

For western blotting experiments, after urea washing, beads were equilibrated in mild lysis buffer. Elution was performed by incubating the beads 15min at 23°C, 15min at 95°C in 30μl 2.5X Laemlli buffer supplemented with 10mM biotin and 20mM DTT. The eluate was brought down to 1X concentration with lysis buffer prior to western blotting. We note that detection of total biotinylated species by western blot was extremely sensitive to detection conditions. Membranes were blocked for 10min in PBS, 2.5%BSA, 0.4% Triton-X 100. 1ng/ml streptavidin-HRP in blocking buffer was added for 25min at room temperature. The membrane was washed for 15min in PBS 0.4% TritonX-100 prior to ECL exposure.

To measure BioID activity after indisulam treatment, cells were treated for 48hrs with 0.1μm indisulam, followed by 24hrs in indisulam with 50μm biotin and 5μm MG132.

Proteomic analysis of DCAF15 interaction partners

For proteomics experiments, after the urea buffer washes, the samples were resuspended in denaturing buffer (8M urea, 50 mM ammonium bicarbonate pH 7.8). Proteins were reduced with dithiothreitol (5 mM, RT, 30min) and alkylated with iodoacetamide (15 mM RT, 45 min in the dark). Excess iodoacetamide was quenched with dithiothreitol (5 mM, room temperature, 20 min

in the dark). The samples were diluted to 1 M urea using 50 mM ammonium bicarbonate and then digested with trypsin (37°C, 16h). After protein digestion, samples were acidified with trifluoroacetic acid to a final concentration of 0.5% and desalted using C18 StageTips [71]. Peptides were eluted with 40% acetonitrile/5% formic acid then 80% acetonitrile/5% formic acid and dried overnight under vacuum at 25°C (Labconco CentriVap Benchtop Vacuum Concentrator, Kansas City, Mo).

For tandem mass tag (TMT) labeling, dried peptides were resuspended in 50µL 200mM HEPES/30% anhydrous acetonitrile. TMT reagents (5 mg) were dissolved in anhydrous acetonitrile (250µL) of which 10µL was added to peptides to achieve a final acetonitrile concentration of approximately 30% (v/v). Following incubation at room temperature for 1 h, the reaction was quenched with 5% hydroxylamine/200mM HEPES to a final concentration of 0.3% (v/v). The TMT labeled peptides were acidified with 50µL 1% trifluoroacetic acid and pooled prior to desalting with SepPak (Waters) and dried under vacuum.

The pooled TMT-labeled peptides were fractionated using high pH RP-HPLC. The samples were resuspended in 5% formic acid/5% acetonitrile and fractionated over a ZORBAX extended C18 column (Agilent, 5µm particles, 4.6 mm ID and 250 mm in length). Peptides were separated on a 75-min linear gradient from 5% to 35% acetonitrile in 10mM ammonium bicarbonate at a flow rate of 0.5mL/min on an Agilent 1260 Infinity pump equipped with a degasser and a diode array detector (set at 214, 220, and 254nm wavelength) from Agilent Technologies (Waldbronn, Germany). The samples were fractionated into a total of 96 fractions and then consolidated into 12 as described previously [72]. Samples were dried down under vacuum and reconstituted in 4% acetonitrile/5% formic acid for LC-MS/MS processing.

Peptides were analyzed on an Orbitrap Fusion Lumos mass spectrometer (Thermo Fisher Scientific) coupled to an Easy-nLC (Thermo Fisher Scientific). Peptides were separated on a microcapillary column (100 µm internal diameter, 25 cm long, filled using Maccel C18 AQ resin, 1.8µm, 120A; Sepax Technologies). The total LC-MS run length for each sample was 180 min comprising a 165 min gradient from 6 to 30% acetonitrile in 0.125% formic acid. The flow rate was 300 nL/min and the column was heated to 60°C.

Data-dependent acquisition (DDA) mode was used for mass spectrometry data collection. A high resolution MS1 scan in the Orbitrap (m/z range 500-1,200, 60k resolution, AGC 5 x 10^5, max injection time 100 ms, RF for S-lens 30) was collected from which the top 10 precursors were selected for MS2 analysis followed by MS3 analysis. For MS2 spectra, ions were isolated using a 0.5 m/z window using the mass filter. The MS2 scan was performed in the quadrupole ion trap (CID, AGC 1 x 10^4, normalized collision energy 30%, max injection time 35 ms) and the MS3 scan was analyzed in the Orbitrap (HCD, 60k resolution, max AGC 5x10^4, max injection time 250 ms, normalized collision energy 50). For TMT reporter ion quantification, up to six fragment ions from each MS2 spectrum were selected for MS3 analysis using synchronous precursor selection (SPS).

Mass spectrometry data were processed using an in-house software pipeline [73]. Raw files were converted to mzXML files and searched against a composite human uniprot database (downloaded on 29th March 2017) containing sequences in forward and reverse orientations using the Sequest algorithm. Database searching matched MS/MS spectra with fully tryptic peptides from this composite dataset with a precursor ion tolerance of 20 ppm and a product ion tolerance of 0.6 Da. Carbamidomethylation of cysteine residues (+57.02146 Da) and TMT tags of peptide N-termini (+229.162932 Da) were set as static modifications. Oxidation of methionines (+15.99492 Da) was set as a variable modification. Linear discriminant analysis was used to filter peptide spectral matches to a 1 % FDR (false discovery rate) as described previously [73]. Non-unique peptides that matched to multiple proteins were assigned to proteins that contained the largest number of matched redundant peptides sequences using the principle of Occam's razor [73].

Quantification of TMT reporter ion intensities was performed by extracting the most intense ion within a 0.003 m/z window at the predicted m/z value for each reporter ion. TMT spectra were used for quantification when the sum of the signal-to-noise for all the reporter ions was greater than 200 and the isolation specificity was greater than 0.75 [74].

Base 2 logarithm of protein fold-changes were estimated by fitting a previously described Bayesian model [75] to the peptide level intensities. Protein estimates are reported as the mean of the posterior

distribution for each parameter. Similarly, coefficients of variation are calculated by taking the posterior variance divided by the posterior mean. The probability of a small change ("P_null") was estimated as the frequency of posterior samples that fall within the interval (-1,1) on the log2 scale.

Polyubiquitination assay

Experiments were performed as per [76]. One million 293Ts were plated in 6-well dishes overnight. Cells were transfected with 500ng of plasmids containing CMV-6his-ubiquitin, CMV-3fl-EGFP, EF1A-DCAF15-3fl and/or CMV-SMC1A-HA. The SMC1A open reading frame was synthesized based on reference sequence NM_006306.3. After 36hrs, cells were treated with 2μM indisulam and/or 10μM MG132. 12hrs later, replicate wells were harvested for whole-cell lysates or for Ni-NTA pulldowns. Whole-cell lysates were made by extraction in 500μl NP40 lysis buffer. For Ni-NTA pulldowns, cells were solubilized in 700μl of guanidine buffer (6M guanidine-HCL, 0.1M Na_2HPO_4/NaH_2PO_4, 10mM imidazole, 0.05% TWEEN 20, pH 8.0), run through QIAshredder columns (Qiagen) and briefly sonicated. Purifications of 6his-ubiquinated species were performed as described in [76], except for the use of magnetic Ni-NTA beads (Thermo Fisher Scientific 88831) and the addition of 0.05% TWEEN 20 to wash buffers.

Data processing

Unless otherwise specified, data was graphed and statistically analyzed using Prism (GraphPad Software). Sample size was not predetermined, No outliers were excluded. Unless otherwise noted, all data points represent biological replicates rather than technical replicates. We define 'technical replicates' as running an assay multiple times on the exact same sample.

Acknowledgements

We thank Jonathan Paw for flow cytometry and cell sorting; Margaret Roy, Andrea Ireland, Twaritha Vijay, Nicole Fong for next-generation sequencing; Adam Baker and Matt Sooknah for RNA-seq data visualization; Hugo Hilton, David Stokoe, and Robert Cohen for critical reading of the manuscript, and members of the Calico Oncology group for helpful discussion.

Competing Interests

All authors are employees of Calico Life Sciences, LLC.

References

1 Snyder, A. *et al.* Genetic basis for clinical response to CTLA-4 blockade in melanoma. *N Engl J Med* **371**, 2189-2199, doi:10.1056/NEJMoa1406498 (2014).

2 Tumeh, P. C. *et al.* PD-1 blockade induces responses by inhibiting adaptive immune resistance. *Nature* **515**, 568-571, doi:10.1038/nature13954 (2014).

3 Mariathasan, S. *et al.* TGFbeta attenuates tumour response to PD-L1 blockade by contributing to exclusion of T cells. *Nature* **554**, 544-548, doi:10.1038/nature25501 (2018).

4 Galon, J. & Bruni, D. Approaches to treat immune hot, altered and cold tumours with combination immunotherapies. *Nat Rev Drug Discov*, doi:10.1038/s41573-018-0007-y (2019).

5 Easwaran, H., Tsai, H. C. & Baylin, S. B. Cancer epigenetics: tumor heterogeneity, plasticity of stem-like states, and drug resistance. *Mol Cell* **54**, 716-727, doi:10.1016/j.molcel.2014.05.015 (2014).

6 Zaretsky, J. M. *et al.* Mutations Associated with Acquired Resistance to PD-1 Blockade in Melanoma. *N Engl J Med* **375**, 819-829, doi:10.1056/NEJMoa1604958 (2016).

7 Sade-Feldman, M. *et al.* Resistance to checkpoint blockade therapy through inactivation of antigen presentation. *Nat Commun* **8**, 1136, doi:10.1038/s41467-017-01062-w (2017).

8 Kearney, C. J. *et al.* Tumor immune evasion arises through loss of TNF sensitivity. *Sci Immunol* **3**, doi:10.1126/sciimmunol.aar3451 (2018).

9 Pan, D. *et al.* A major chromatin regulator determines resistance of tumor cells to T cell-mediated killing. *Science* **359**, 770-775, doi:10.1126/science.aao1710 (2018).

10 Manguso, R. T. *et al.* In vivo CRISPR screening identifies Ptpn2 as a cancer immunotherapy target. *Nature* **547**, 413-418, doi:10.1038/nature23270 (2017).

11 Patel, S. J. *et al.* Identification of essential genes for cancer immunotherapy. *Nature* **548**, 537-542, doi:10.1038/nature23477 (2017).

12 Dunn, G. P., Old, L. J. & Schreiber, R. D. The immunobiology of cancer immunosurveillance and immunoediting. *Immunity* **21**, 137-148, doi:10.1016/j.immuni.2004.07.017 (2004).

13 Rodig, S. J. *et al.* MHC proteins confer differential sensitivity to CTLA-4 and PD-1 blockade in untreated metastatic melanoma. *Sci Transl Med* **10**, doi:10.1126/scitranslmed.aar3342 (2018).

14 Gao, J. *et al.* Loss of IFN-gamma Pathway Genes in Tumor Cells as a Mechanism of Resistance to Anti-CTLA-4 Therapy. *Cell* **167**, 397-404 e399, doi:10.1016/j.cell.2016.08.069 (2016).

15 McGranahan, N. *et al.* Allele-Specific HLA Loss and Immune Escape in Lung Cancer Evolution. *Cell* **171**, 1259-1271 e1211, doi:10.1016/j.cell.2017.10.001 (2017).

16 Marcus, A. *et al.* Recognition of tumors by the innate immune system and natural killer cells. *Adv Immunol* **122**, 91-128, doi:10.1016/B978-0-12-800267-4.00003-1 (2014).

17 Moynihan, K. D. *et al.* Eradication of large established tumors in mice by combination immunotherapy that engages innate and adaptive immune responses. *Nat Med* **22**, 1402-1410, doi:10.1038/nm.4200 (2016).

18 Lopez-Soto, A., Gonzalez, S., Smyth, M. J. & Galluzzi, L. Control of Metastasis by NK Cells. *Cancer Cell* **32**, 135-154, doi:10.1016/j.ccell.2017.06.009 (2017).

19 Chiossone, L., Dumas, P. Y., Vienne, M. & Vivier, E. Natural killer cells and other innate lymphoid cells in cancer. *Nat Rev Immunol* **18**, 671-688, doi:10.1038/s41577-018-0061-z (2018).

20 Ljunggren, H. G. & Malmberg, K. J. Prospects for the use of NK cells in immunotherapy of human cancer. *Nat Rev Immunol* **7**, 329-339, doi:10.1038/nri2073 (2007).

21 Klingemann, H. G. *et al.* Establishment and characterization of a human leukemic cell line (SR-91) with features suggestive of early hematopoietic progenitor cell origin. *Leuk Lymphoma* **12**, 463-470, doi:10.3109/10428199409073789 (1994).

22 Maki, G., Klingemann, H. G., Martinson, J. A. & Tam, Y. K. Factors regulating the cytotoxic activity of the human natural killer cell line, NK-92. *J Hematother Stem Cell Res* **10**, 369-383, doi:10.1089/152581601750288975 (2001).

23 Li, W. *et al.* MAGeCK enables robust identification of essential genes from genome-scale CRISPR/Cas9 knockout screens. *Genome Biol* **15**, 554, doi:10.1186/s13059-014-0554-4 (2014).

24 Brandt, C. S. *et al.* The B7 family member B7-H6 is a tumor cell ligand for the activating natural killer cell receptor NKp30 in humans. *J Exp Med* **206**, 1495-1503, doi:10.1084/jem.20090681 (2009).

25 Selvaraj, P. *et al.* The T lymphocyte glycoprotein CD2 binds the cell surface ligand LFA-3. *Nature* **326**, 400-403, doi:10.1038/326400a0 (1987).

26 Rolle, A. *et al.* CD2-CD58 interactions are pivotal for the activation and function of adaptive natural killer cells in human cytomegalovirus infection. *Eur J Immunol* **46**, 2420-2425, doi:10.1002/eji.201646492 (2016).

27 Martin, M. *et al.* CD84 functions as a homophilic adhesion molecule and enhances IFN-gamma secretion: adhesion is mediated by Ig-like domain 1. *J Immunol* **167**, 3668-3676 (2001).

28 Veillette, A. Immune regulation by SLAM family receptors and SAP-related adaptors. *Nat Rev Immunol* **6**, 56-66, doi:10.1038/nri1761 (2006).

29 Wang, N. *et al.* Cutting edge: The adapters EAT-2A and -2B are positive regulators of CD244- and CD84-dependent NK cell functions in the C57BL/6 mouse. *J Immunol* **185**, 5683-5687, doi:10.4049/jimmunol.1001974 (2010).

30 Stanietsky, N. *et al.* The interaction of TIGIT with PVR and PVRL2 inhibits human NK cell cytotoxicity. *Proc Natl Acad Sci U S A* **106**, 17858-17863, doi:10.1073/pnas.0903474106 (2009).

31 Bottino, C. *et al.* Identification of PVR (CD155) and Nectin-2 (CD112) as cell surface ligands for the human DNAM-1 (CD226) activating molecule. *J Exp Med* **198**, 557-567, doi:10.1084/jem.20030788 (2003).

32 Jin, J., Arias, E. E., Chen, J., Harper, J. W. & Walter, J. C. A family of diverse Cul4-Ddb1-interacting proteins includes Cdt2, which is required for S phase destruction of the replication factor Cdt1. *Mol Cell* **23**, 709-721, doi:10.1016/j.molcel.2006.08.010 (2006).

33 Jackson, S. & Xiong, Y. CRL4s: the CUL4-RING E3 ubiquitin ligases. *Trends Biochem Sci* **34**, 562-570, doi:10.1016/j.tibs.2009.07.002 (2009).

34 Uhlmann, F. SMC complexes: from DNA to chromosomes. *Nat Rev Mol Cell Biol* **17**, 399-412, doi:10.1038/nrm.2016.30 (2016).

35 Mazumdar, C. & Majeti, R. The role of mutations in the cohesin complex in acute myeloid leukemia. *Int J Hematol* **105**, 31-36, doi:10.1007/s12185-016-2119-7 (2017).

36 Chen, E., Karr, R. W., Frost, J. P., Gonwa, T. A. & Ginder, G. D. Gamma interferon and 5-azacytidine cause transcriptional elevation of class I major histocompatibility complex gene expression in K562 leukemia cells in the absence of differentiation. *Mol Cell Biol* **6**, 1698-1705 (1986).

37 Chen, L. & Flies, D. B. Molecular mechanisms of T cell co-stimulation and co-inhibition. *Nat Rev Immunol* **13**, 227-242, doi:10.1038/nri3405 (2013).

38 Acuto, O. & Michel, F. CD28-mediated co-stimulation: a quantitative support for TCR signalling. *Nat Rev Immunol* **3**, 939-951, doi:10.1038/nri1248 (2003).

39 Lindner, I. *et al.* Induced dendritic cell differentiation of chronic myeloid leukemia blasts is associated with down-regulation of BCR-ABL. *J Immunol* **171**, 1780-1791 (2003).

40 Townsend, S. E. & Allison, J. P. Tumor rejection after direct costimulation of CD8+ T cells by B7-transfected melanoma cells. *Science* **259**, 368-370 (1993).

41 Chen, L. *et al.* Costimulation of antitumor immunity by the B7 counterreceptor for the T lymphocyte molecules CD28 and CTLA-4. *Cell* **71**, 1093-1102 (1992).

42 Wilson, J. L. *et al.* NK cell triggering by the human costimulatory molecules CD80 and CD86. *J Immunol* **163**, 4207-4212 (1999).

43 Galea-Lauri, J. *et al.* Expression of a variant of CD28 on a subpopulation of human NK cells: implications for B7-mediated stimulation of NK cells. *J Immunol* **163**, 62-70 (1999).

44 Chambers, B. J., Salcedo, M. & Ljunggren, H. G. Triggering of natural killer cells by the costimulatory molecule CD80 (B7-1). *Immunity* **5**, 311-317 (1996).

45 Azuma, M., Cayabyab, M., Buck, D., Phillips, J. H. & Lanier, L. L. Involvement of CD28 in MHC-unrestricted cytotoxicity mediated by a human natural killer leukemia cell line. *J Immunol* **149**, 1115-1123 (1992).

46 Martin-Fontecha, A., Assarsson, E., Carbone, E., Karre, K. & Ljunggren, H. G. Triggering of murine NK cells by CD40 and CD86 (B7-2). *J Immunol* **162**, 5910-5916 (1999).

47 Peach, R. J. *et al.* Both extracellular immunoglobin-like domains of CD80 contain residues critical for binding T cell surface receptors CTLA-4 and CD28. *J Biol Chem* **270**, 21181-21187 (1995).

48 Assi, R. *et al.* Final results of a phase 2, open-label study of indisulam, idarubicin, and cytarabine in patients with relapsed or refractory acute myeloid leukemia and high-risk myelodysplastic syndrome. *Cancer* **124**, 2758-2765, doi:10.1002/cncr.31398 (2018).

49 Han, T. *et al.* Anticancer sulfonamides target splicing by inducing RBM39 degradation via recruitment to DCAF15. *Science* **356**, doi:10.1126/science.aal3755 (2017).

50 Uehara, T. *et al.* Selective degradation of splicing factor CAPERalpha by anticancer sulfonamides. *Nat Chem Biol* **13**, 675-680, doi:10.1038/nchembio.2363 (2017).

51 Ito, T. *et al.* Identification of a primary target of thalidomide teratogenicity. *Science* **327**, 1345-1350, doi:10.1126/science.1177319 (2010).

52 Fischer, E. S. *et al.* Structure of the DDB1-CRBN E3 ubiquitin ligase in complex with thalidomide. *Nature* **512**, 49-53, doi:10.1038/nature13527 (2014).
53 Kronke, J. *et al.* Lenalidomide causes selective degradation of IKZF1 and IKZF3 in multiple myeloma cells. *Science* **343**, 301-305, doi:10.1126/science.1244851 (2014).
54 Bolouri, H. *et al.* The molecular landscape of pediatric acute myeloid leukemia reveals recurrent structural alterations and age-specific mutational interactions. *Nat Med* **24**, 103-112, doi:10.1038/nm.4439 (2018).
55 Cancer Genome Atlas Research, N. *et al.* Genomic and epigenomic landscapes of adult de novo acute myeloid leukemia. *N Engl J Med* **368**, 2059-2074, doi:10.1056/NEJMoa1301689 (2013).
56 Roux, K. J., Kim, D. I., Raida, M. & Burke, B. A promiscuous biotin ligase fusion protein identifies proximal and interacting proteins in mammalian cells. *J Cell Biol* **196**, 801-810, doi:10.1083/jcb.201112098 (2012).
57 Luo, N. *et al.* Melanoma response to anti-PD-L1 immunotherapy requires JAK1 signaling, but not JAK2. *Oncoimmunology* **7**, e1438106, doi:10.1080/2162402X.2018.1438106 (2018).
58 Ferlazzo, G. & Munz, C. NK cell compartments and their activation by dendritic cells. *J Immunol* **172**, 1333-1339, doi:10.4049/jimmunol.172.3.1333 (2004).
59 O'Connell, B. C. & Harper, J. W. Ubiquitin proteasome system (UPS): what can chromatin do for you? *Curr Opin Cell Biol* **19**, 206-214, doi:10.1016/j.ceb.2007.02.014 (2007).
60 Litwin, I., Pilarczyk, E. & Wysocki, R. The Emerging Role of Cohesin in the DNA Damage Response. *Genes (Basel)* **9**, doi:10.3390/genes9120581 (2018).
61 Chandrashekar, D. S. *et al.* UALCAN: A Portal for Facilitating Tumor Subgroup Gene Expression and Survival Analyses. *Neoplasia* **19**, 649-658, doi:10.1016/j.neo.2017.05.002 (2017).
62 Doench, J. G. *et al.* Optimized sgRNA design to maximize activity and minimize off-target effects of CRISPR-Cas9. *Nat Biotechnol* **34**, 184-191, doi:10.1038/nbt.3437 (2016).
63 Sanjana, N. E., Shalem, O. & Zhang, F. Improved vectors and genome-wide libraries for CRISPR screening. *Nat Methods* **11**, 783-784, doi:10.1038/nmeth.3047 (2014).
64 Grigaite, R., Maneliene, Z. & Janulaitis, A. AarI, a restriction endonuclease from Arthrobacter aurescens SS2-322, which recognizes the novel non-palindromic sequence 5'-CACCTGC(N)4/8-3'. *Nucleic Acids Res* **30**, e123 (2002).
65 Chen, B. *et al.* Dynamic imaging of genomic loci in living human cells by an optimized CRISPR/Cas system. *Cell* **155**, 1479-1491, doi:10.1016/j.cell.2013.12.001 (2013).
66 van Overbeek, M. *et al.* DNA Repair Profiling Reveals Nonrandom Outcomes at Cas9-Mediated Breaks. *Mol Cell* **63**, 633-646, doi:10.1016/j.molcel.2016.06.037 (2016).
67 Stamper, C. C. *et al.* Crystal structure of the B7-1/CTLA-4 complex that inhibits human immune responses. *Nature* **410**, 608-611, doi:10.1038/35069118 (2001).
68 Patro, R., Duggal, G., Love, M. I., Irizarry, R. A. & Kingsford, C. Salmon provides fast and bias-aware quantification of transcript expression. *Nat Methods* **14**, 417-419, doi:10.1038/nmeth.4197 (2017).
69 Pimentel, H., Bray, N. L., Puente, S., Melsted, P. & Pachter, L. Differential analysis of RNA-seq incorporating quantification uncertainty. *Nat Methods* **14**, 687-690, doi:10.1038/nmeth.4324 (2017).

70 Barretina, J. *et al.* The Cancer Cell Line Encyclopedia enables predictive modelling of anticancer drug sensitivity. *Nature* **483**, 603-607, doi:10.1038/nature11003 (2012).

71 Rappsilber, J., Mann, M. & Ishihama, Y. Protocol for micro-purification, enrichment, pre-fractionation and storage of peptides for proteomics using StageTips. *Nat Protoc* **2**, 1896-1906, doi:10.1038/nprot.2007.261 (2007).

72 Edwards, A. & Haas, W. Multiplexed Quantitative Proteomics for High-Throughput Comprehensive Proteome Comparisons of Human Cell Lines. *Methods Mol Biol* **1394**, 1-13, doi:10.1007/978-1-4939-3341-9_1 (2016).

73 Huttlin, E. L. *et al.* A tissue-specific atlas of mouse protein phosphorylation and expression. *Cell* **143**, 1174-1189, doi:10.1016/j.cell.2010.12.001 (2010).

74 Ting, L., Rad, R., Gygi, S. P. & Haas, W. MS3 eliminates ratio distortion in isobaric multiplexed quantitative proteomics. *Nat Methods* **8**, 937-940, doi:10.1038/nmeth.1714 (2011).

75 O'Brien, J. J. *et al.* Compositional Proteomics: Effects of Spatial Constraints on Protein Quantification Utilizing Isobaric Tags. *J Proteome Res* **17**, 590-599, doi:10.1021/acs.jproteome.7b00699 (2018).

76 Lu, G. *et al.* The myeloma drug lenalidomide promotes the cereblon-dependent destruction of Ikaros proteins. *Science* **343**, 305-309, doi:10.1126/science.1244917 (2014).

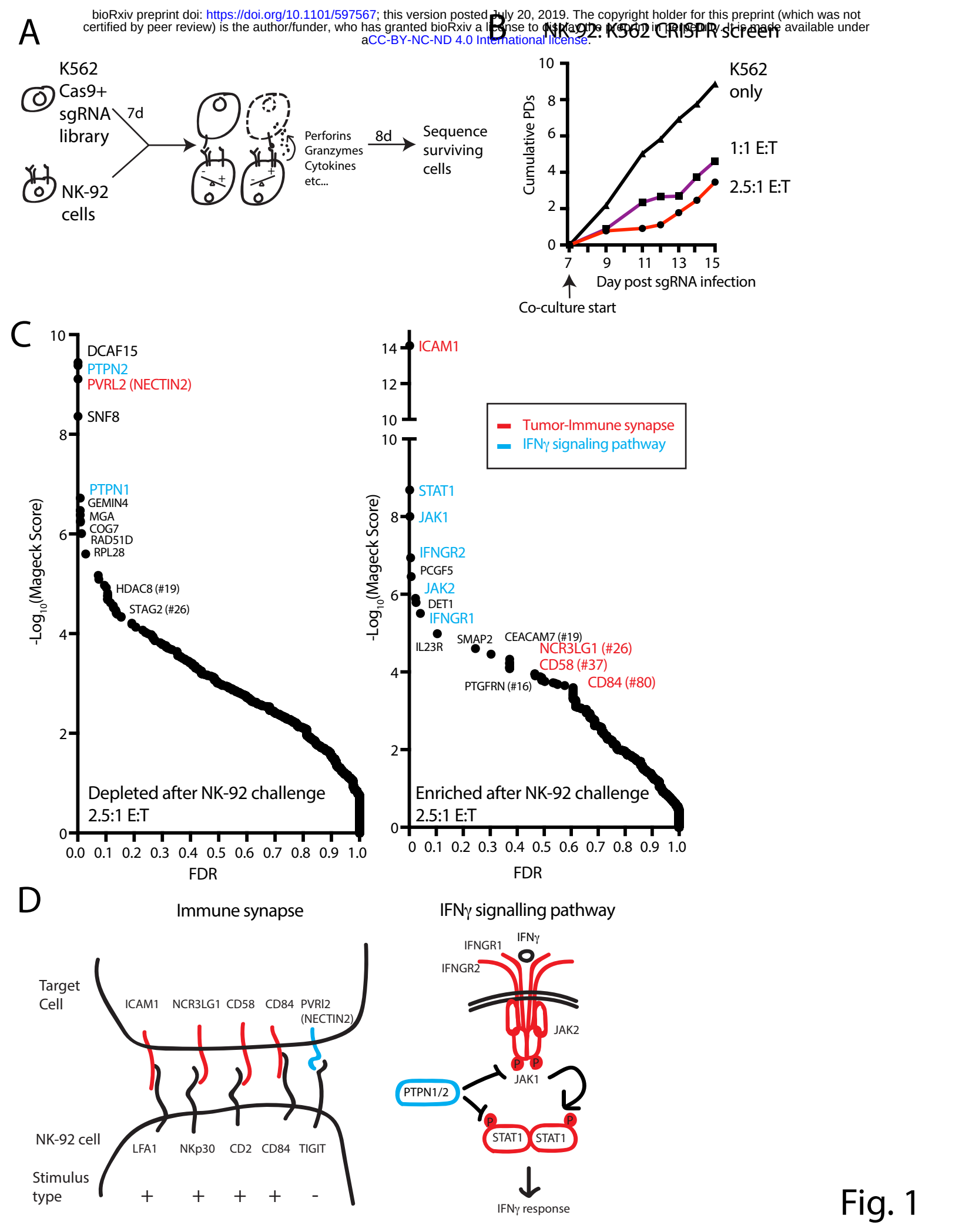

Fig. 1

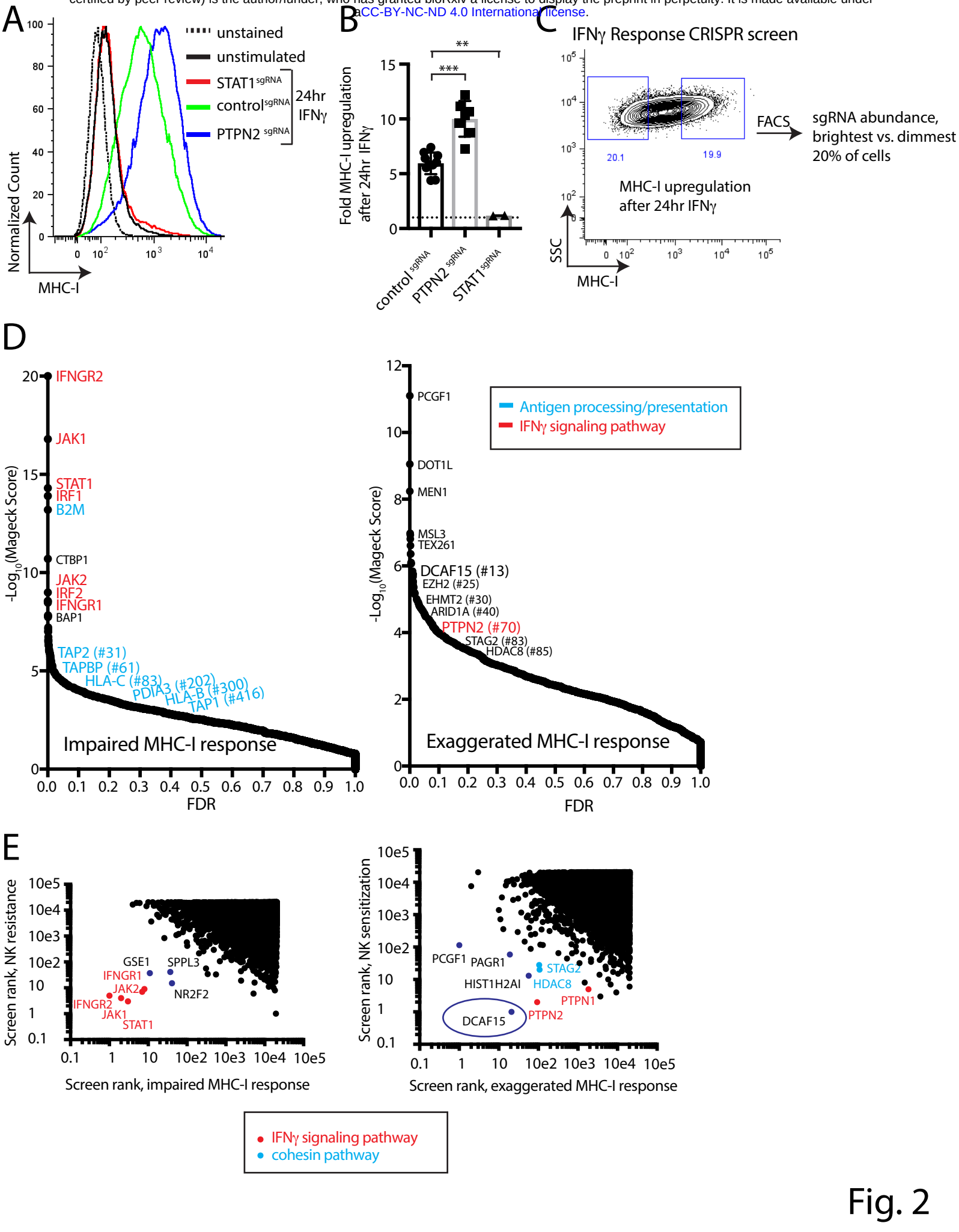

Fig. 2

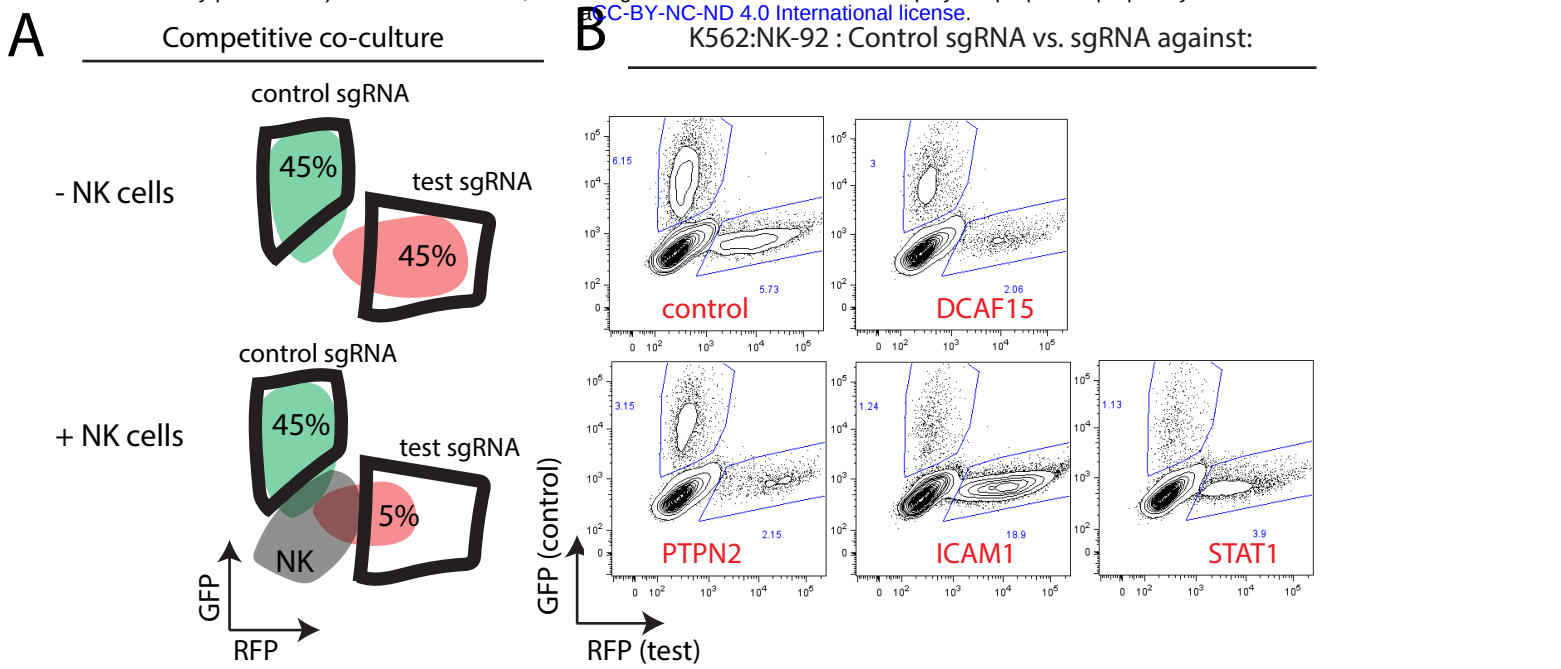

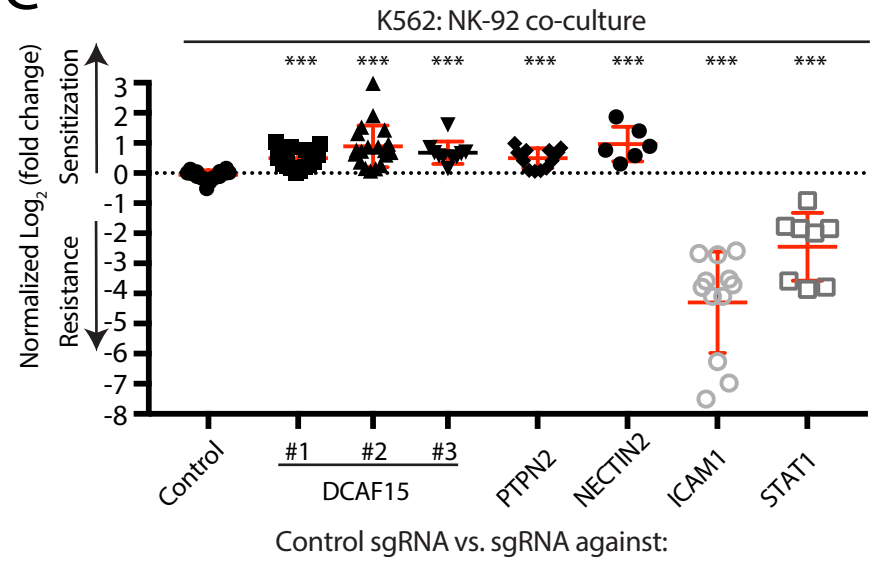

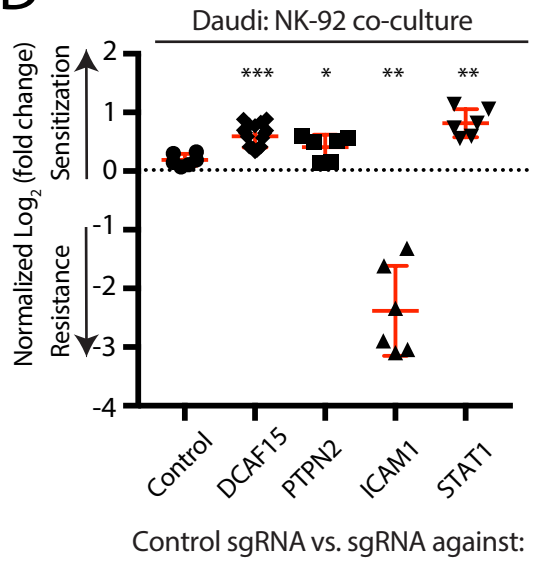

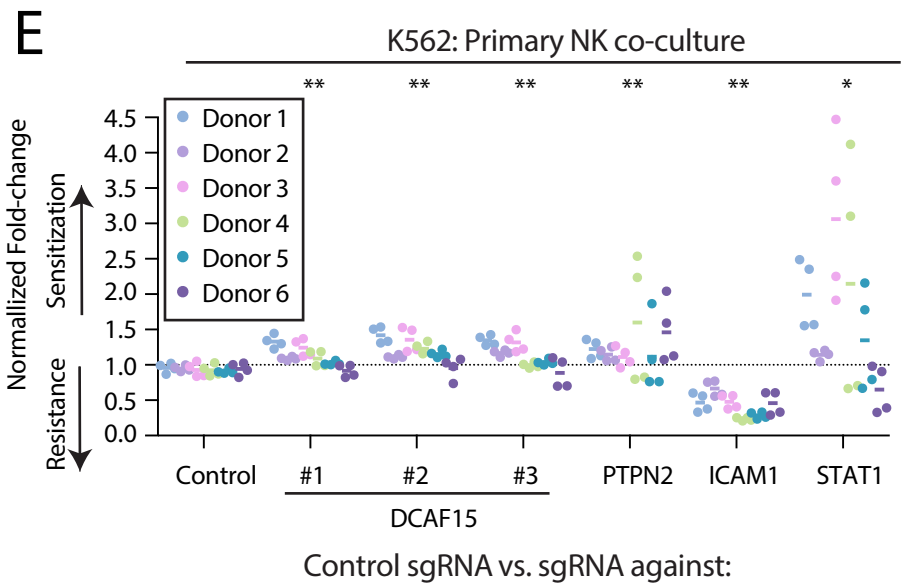

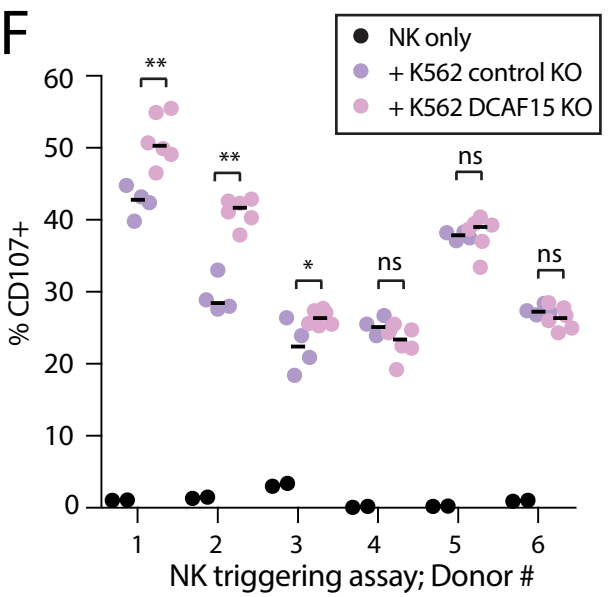

Fig. 3

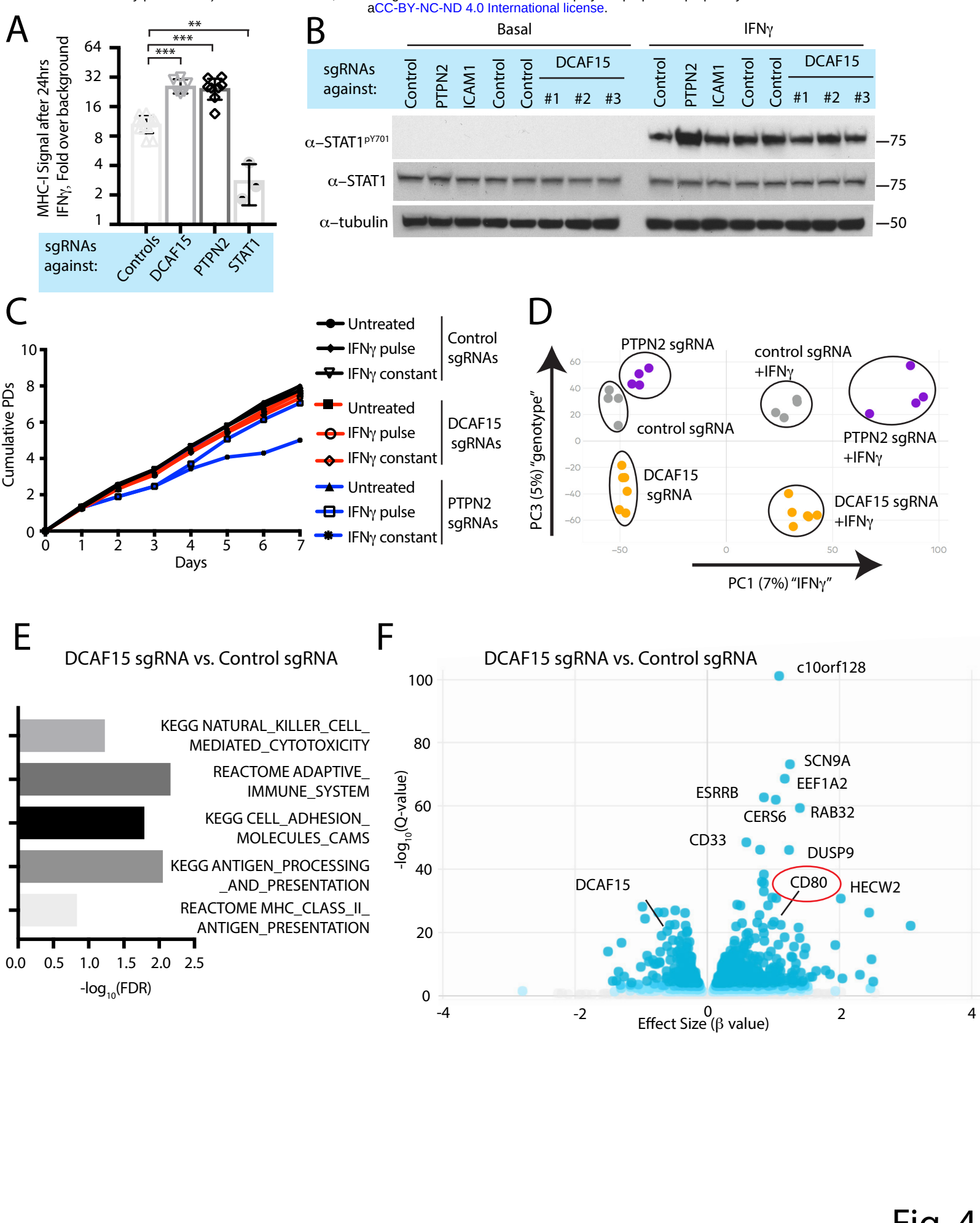

Fig. 4

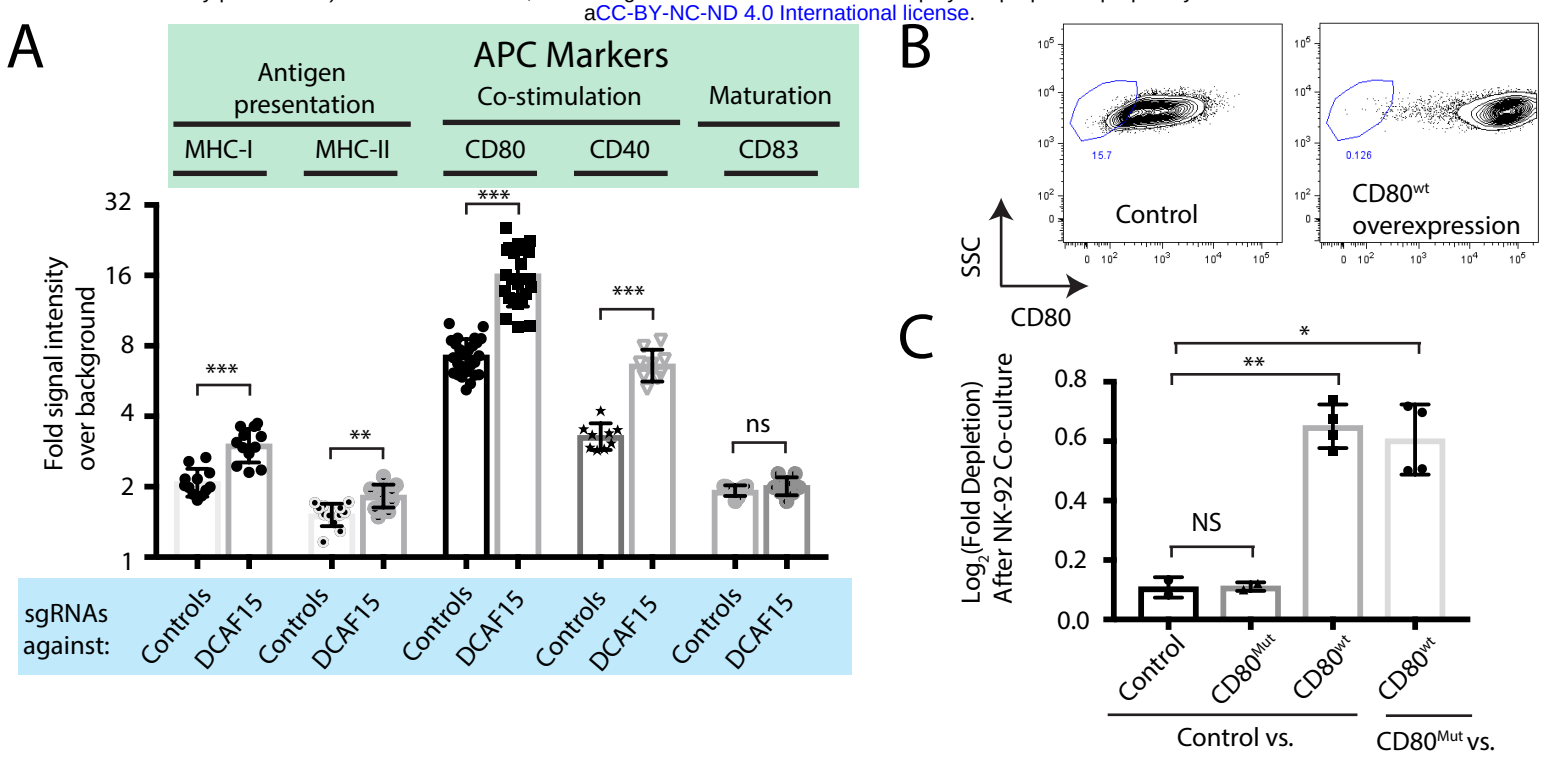

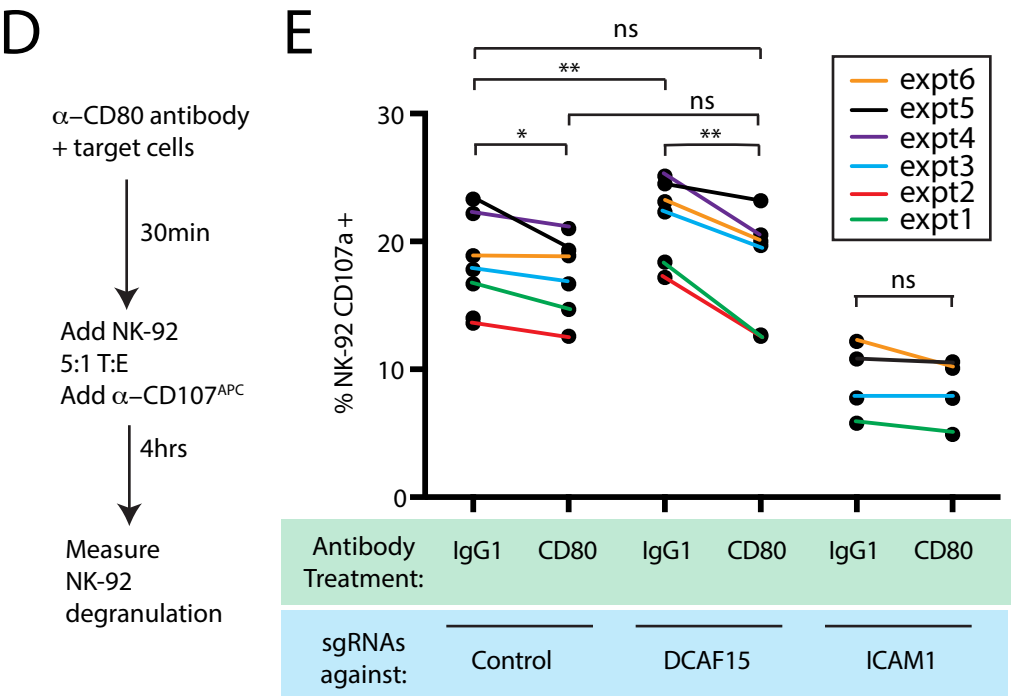

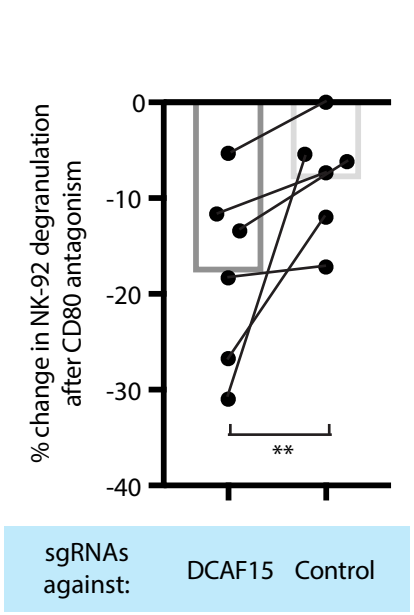

Fig. 5

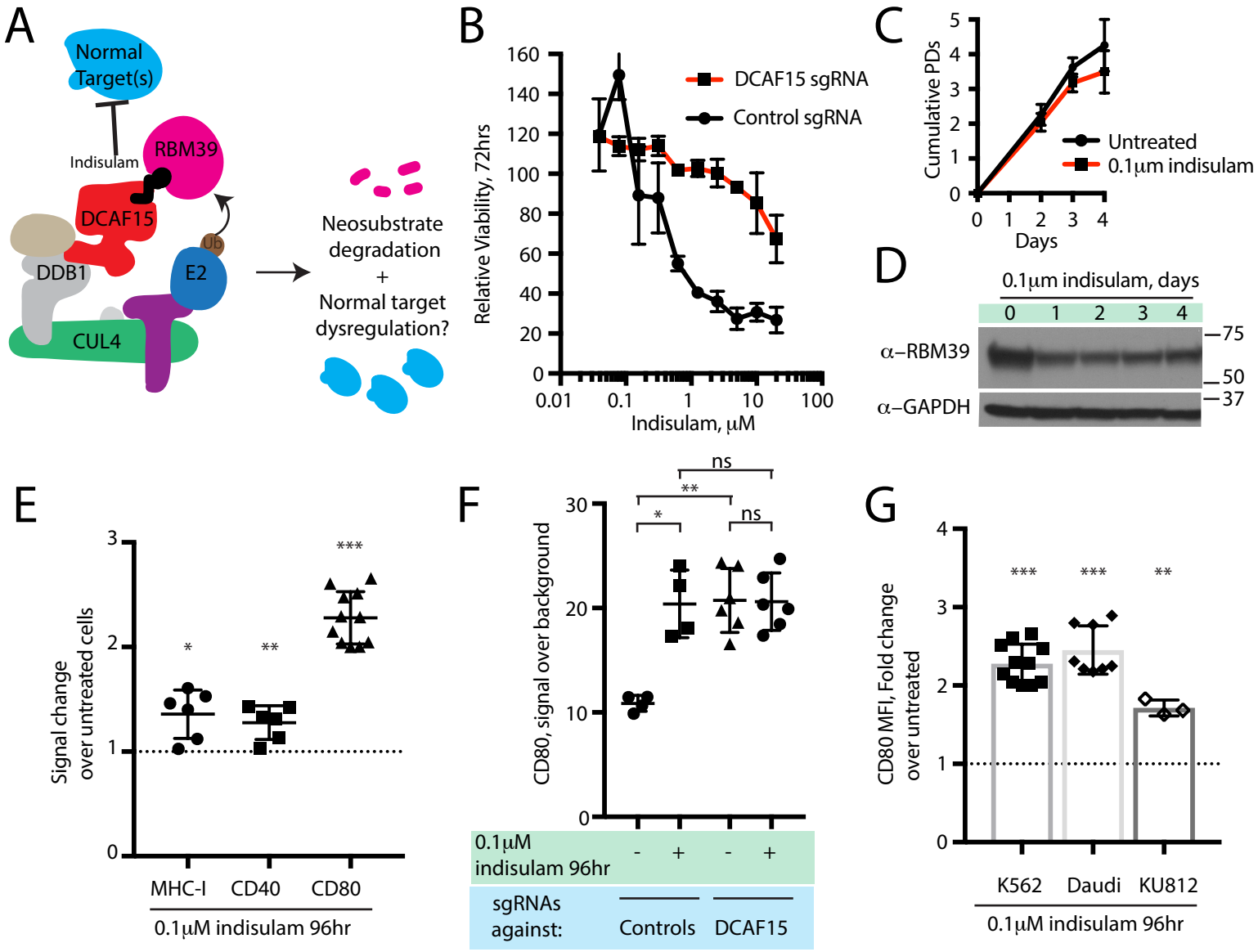

Fig. 6

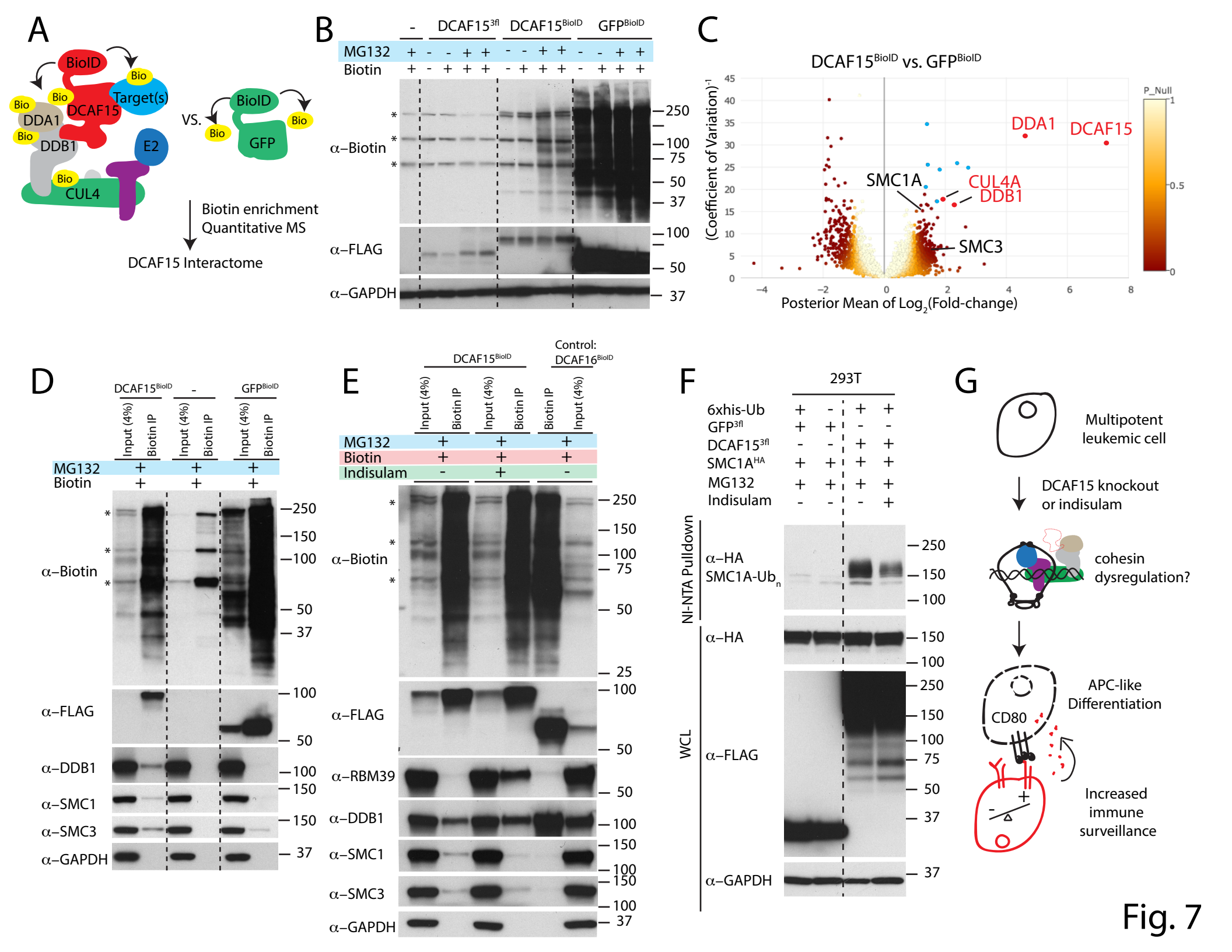
A
BioID
Bio
Target(s)
DCAF15
DDA1
DDB1
E2
CUL4
VS.
GFP
Biotin enrichment
Quantitative MS
DCAF15 Interactome
B
MG132
Biotin
DCAF15 3fl
DCAF15 BioID
GFP BioID
α–Biotin
α–FLAG
α–GAPDH
C
DCAF15 BioID vs. GFP BioID
(Coefficient of Variation)-1
Posterior Mean of Log2(Fold-change)
P_Null
DDA1
DCAF15
SMC1A
CUL4A
DDB1
SMC3
D
DCAF15 BioID
GFP BioID
Input (4%)
Biotin IP
α–Biotin
α–FLAG
α–DDB1
α–SMC1
α–SMC3
α–GAPDH
E
DCAF15 BioID
Control: DCAF16 BioID
Indisulam
α–RBM39
F
293T
6xhis-Ub
GFP 3fl
DCAF15 3fl
SMC1A HA
Indisulam
Ni-NTA Pulldown
WCL
α–HA
SMC1A-Ubn
G
Multipotent leukemic cell
DCAF15 knockout or indisulam
cohesin dysregulation?
APC-like Differentiation
CD80
Increased immune surveillance

Fig. 7

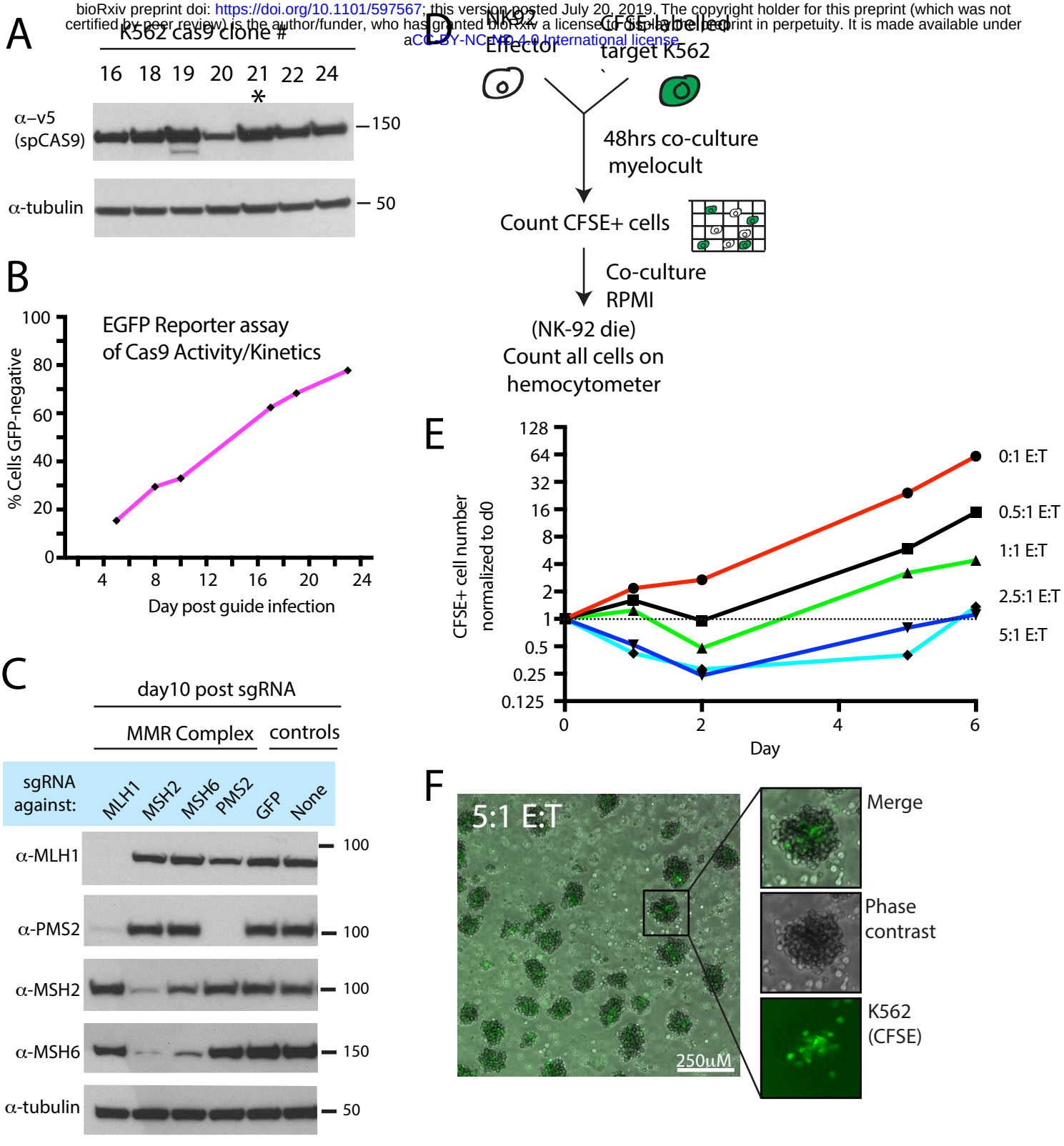

Fig1- S1

A

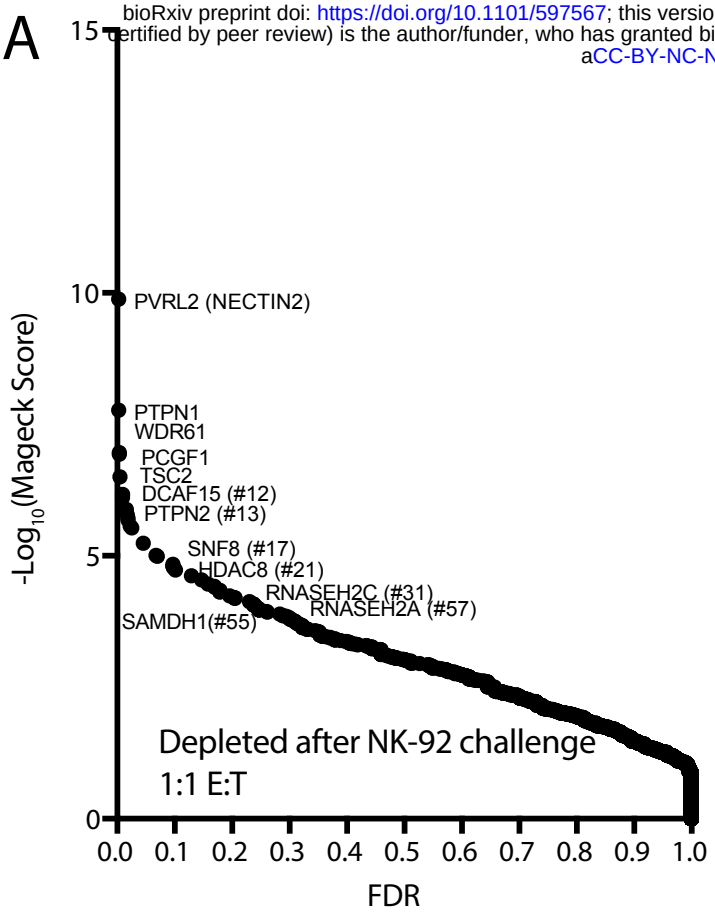

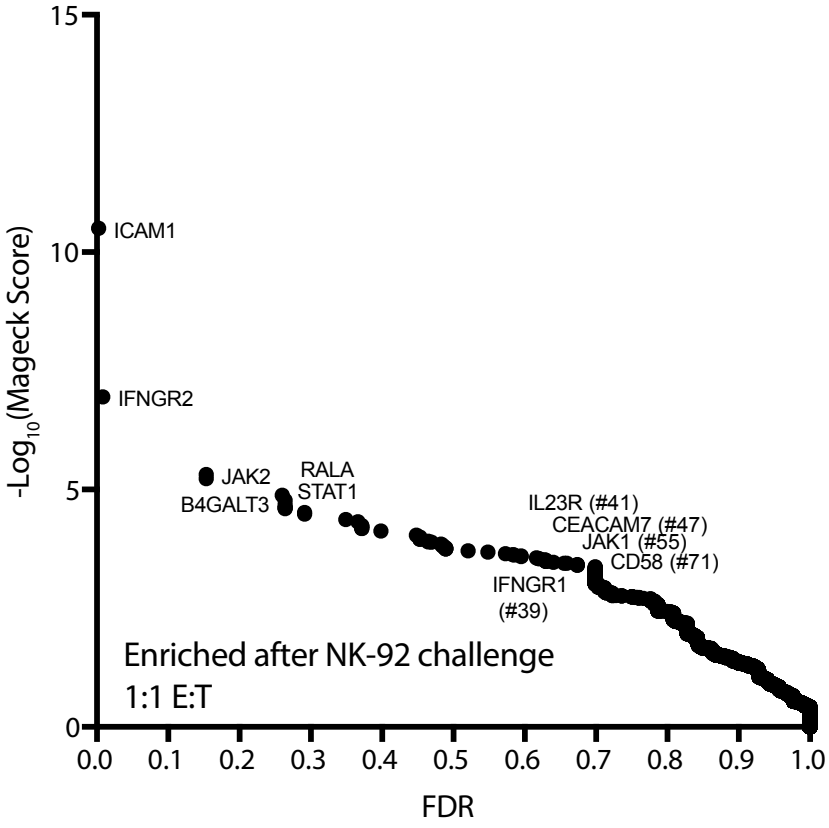

Fig1-S2

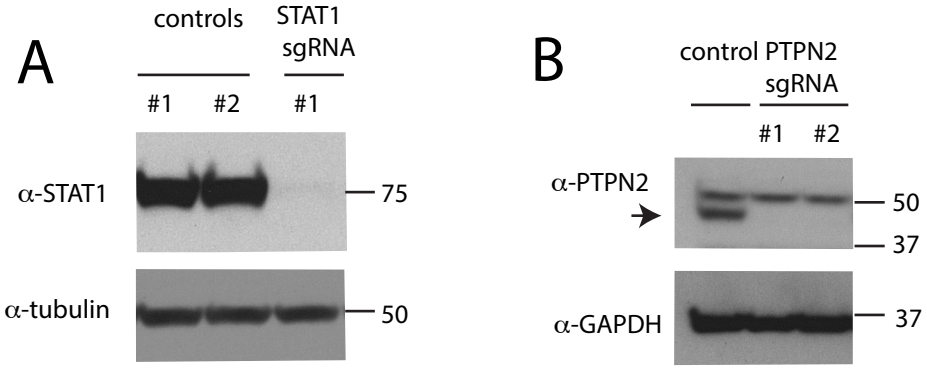

Fig2-S1

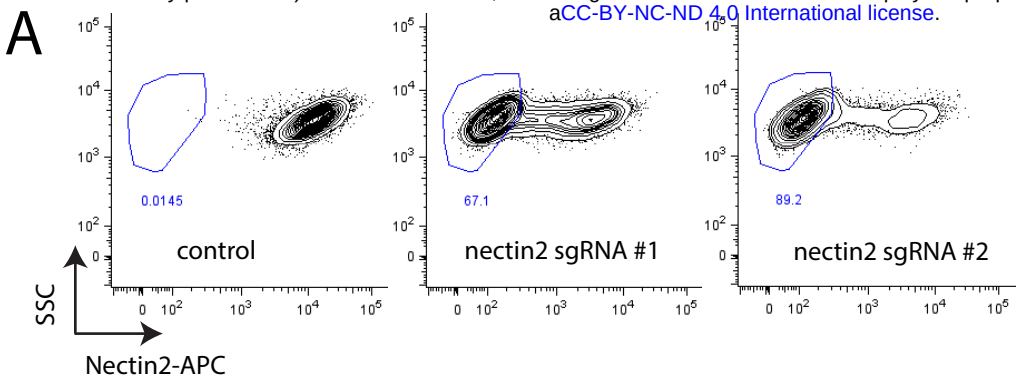

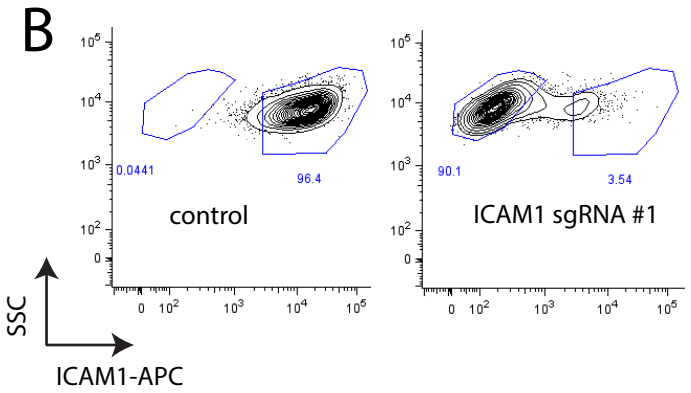

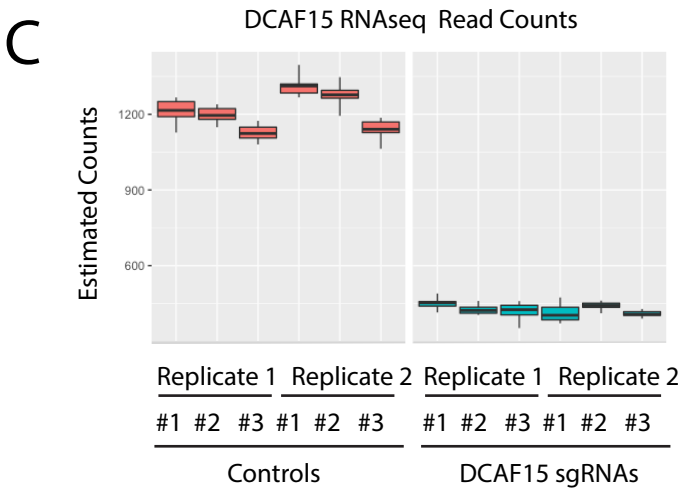

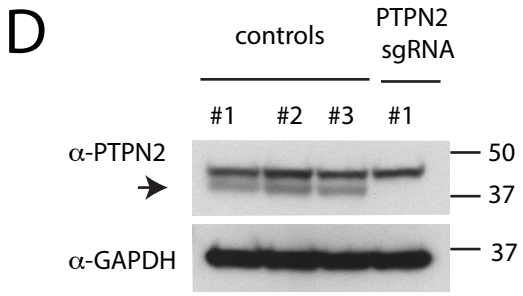

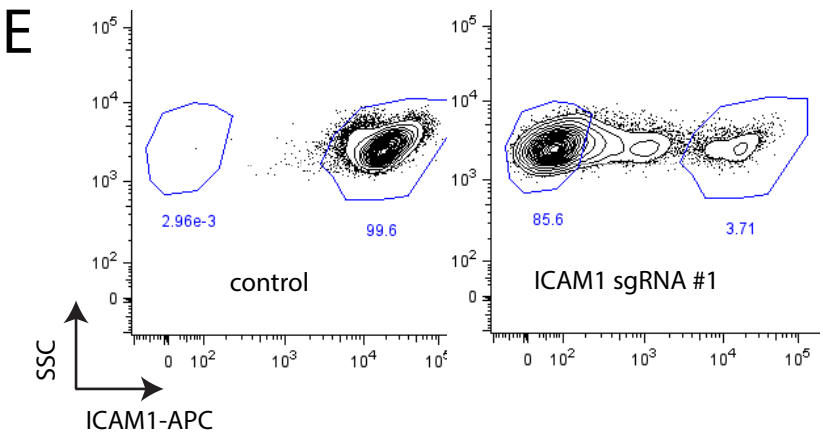

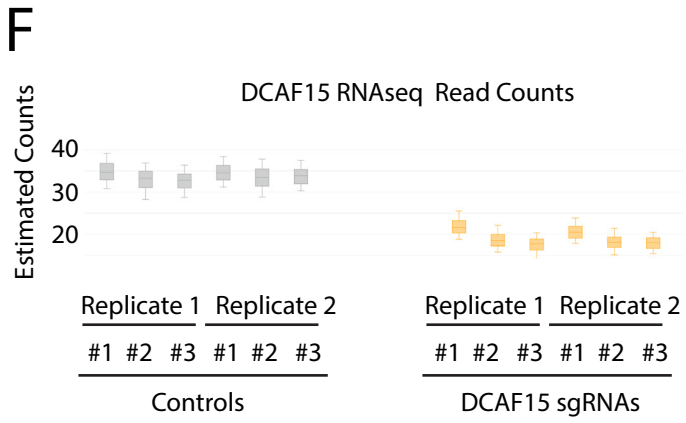

Fig.3-S1

A

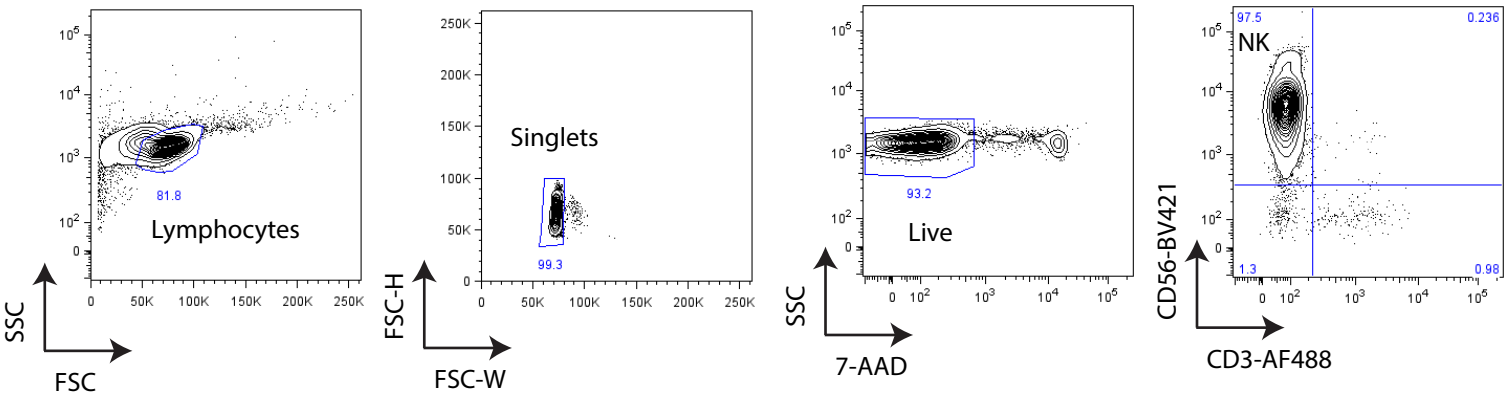

B

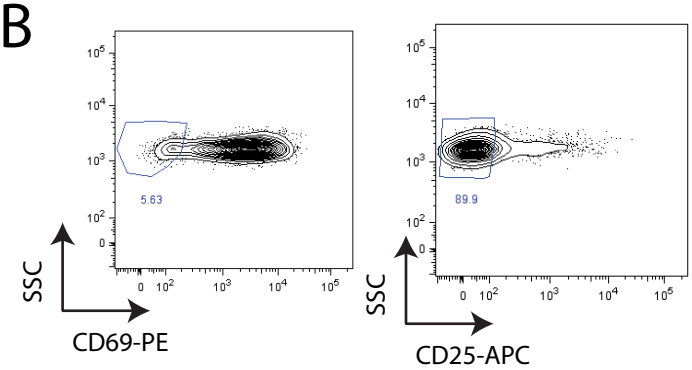

Fig.3-S2

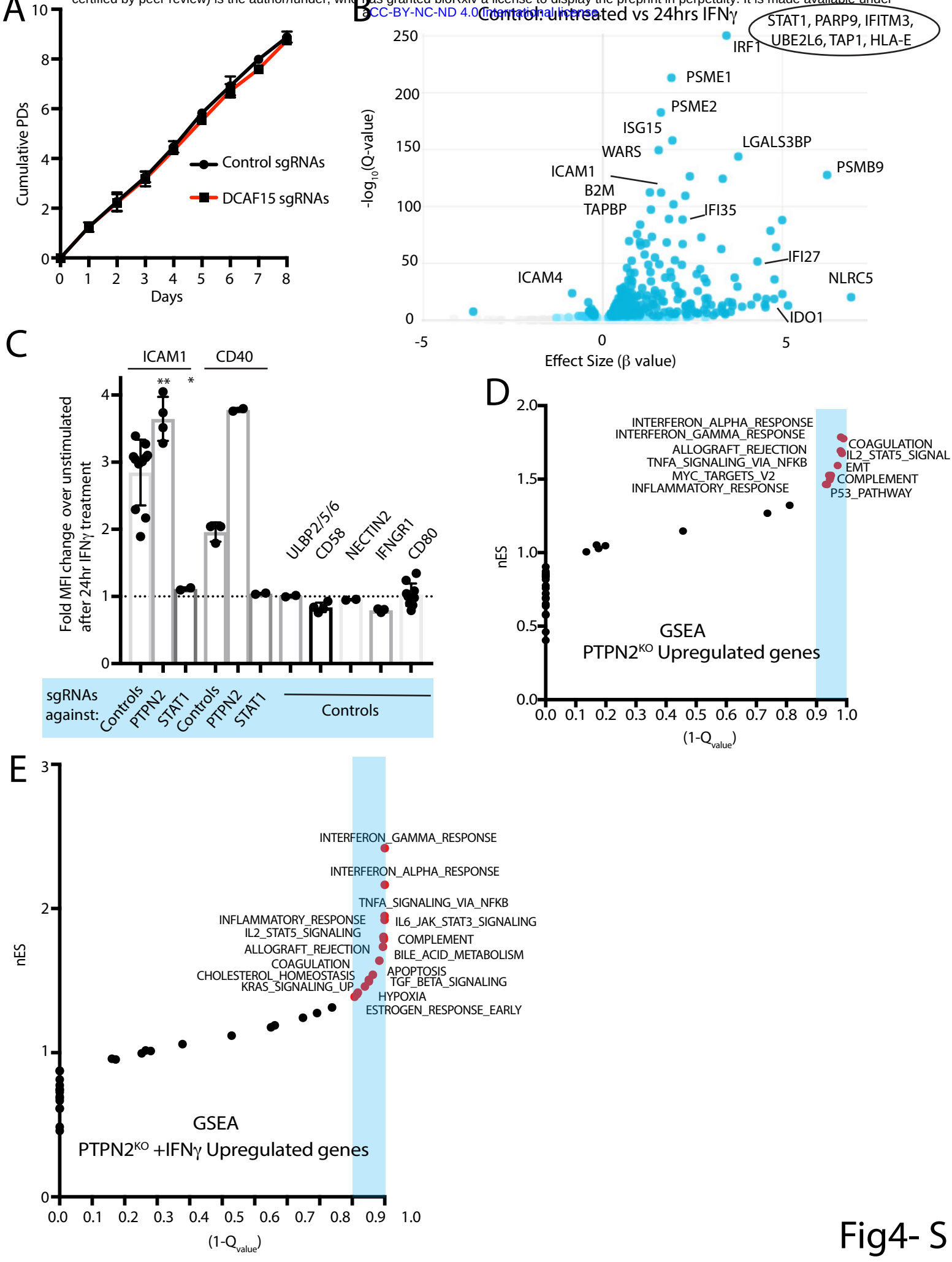

Fig4- S1

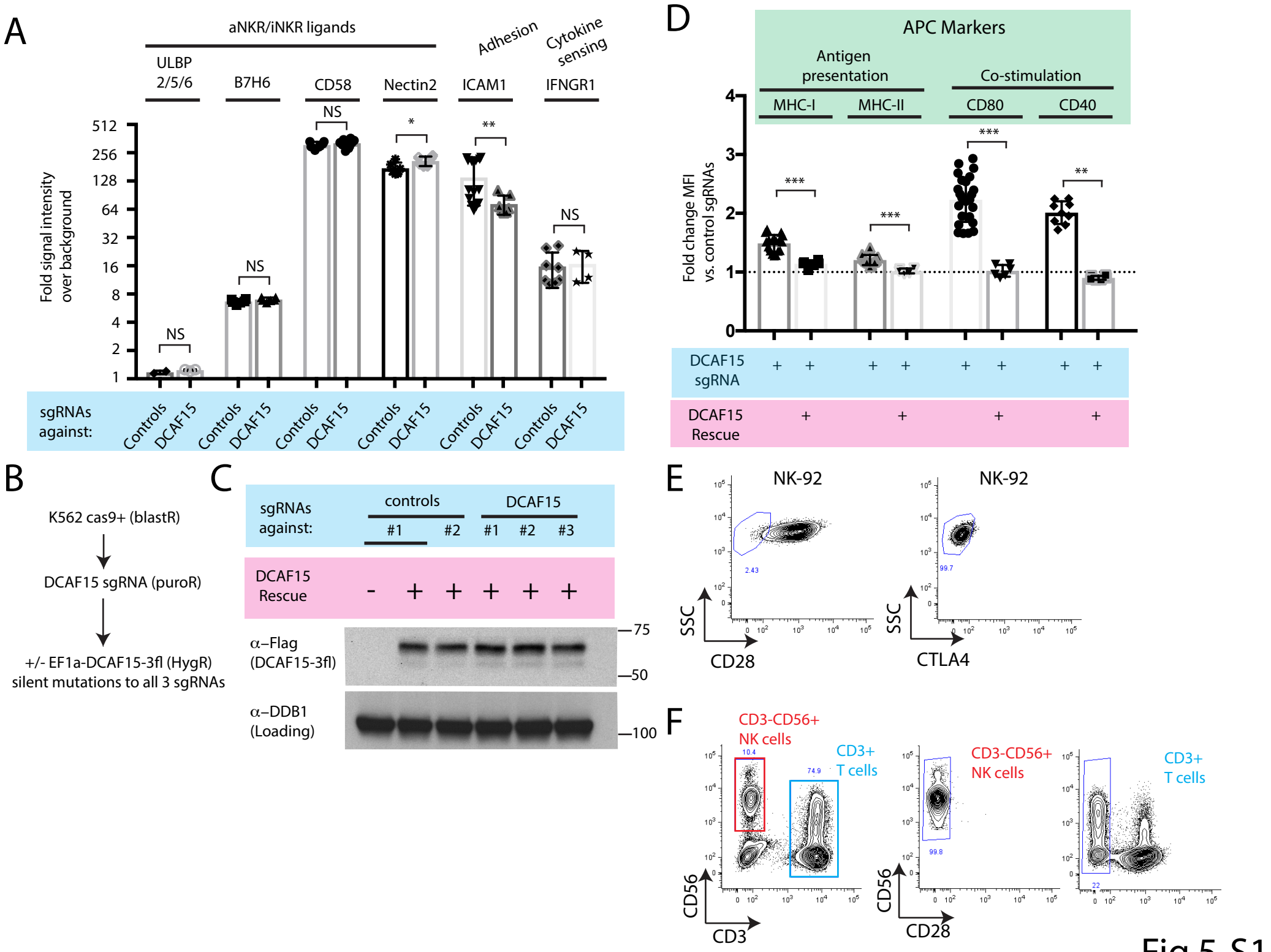
A
aNKR/iNKR ligands
Adhesion
Cytokine sensing
ULBP 2/5/6
B7H6
CD58
Nectin2
ICAM1
IFNGR1
Fold signal intensity over background
512
256
128
64
32
16
8
4
2
1
NS
NS
NS
*
**
NS
sgRNAs against:
Controls
DCAF15
B
K562 cas9+ (blastR)
DCAF15 sgRNA (puroR)
+/- EF1a-DCAF15-3fl (HygR)
silent mutations to all 3 sgRNAs
C
sgRNAs against:
controls
DCAF15
#1
#2
#1
#2
#3
DCAF15 Rescue
- + + + + +
α–Flag (DCAF15-3fl)
α–DDB1 (Loading)
75
50
100
D
APC Markers
Antigen presentation
Co-stimulation
MHC-I
MHC-II
CD80
CD40
Fold change MFI vs. control sgRNAs
4
3
2
1
0
***
***
***
**
DCAF15 sgRNA
DCAF15 Rescue
E
NK-92
NK-92
SSC
CD28
SSC
CTLA4
2.43
99.7
F
CD3-CD56+ NK cells
CD3+ T cells
CD56
CD3
CD3-CD56+ NK cells
CD3+ T cells
CD56
CD28
10.4
74.9
99.8
22

Fig.5-S1

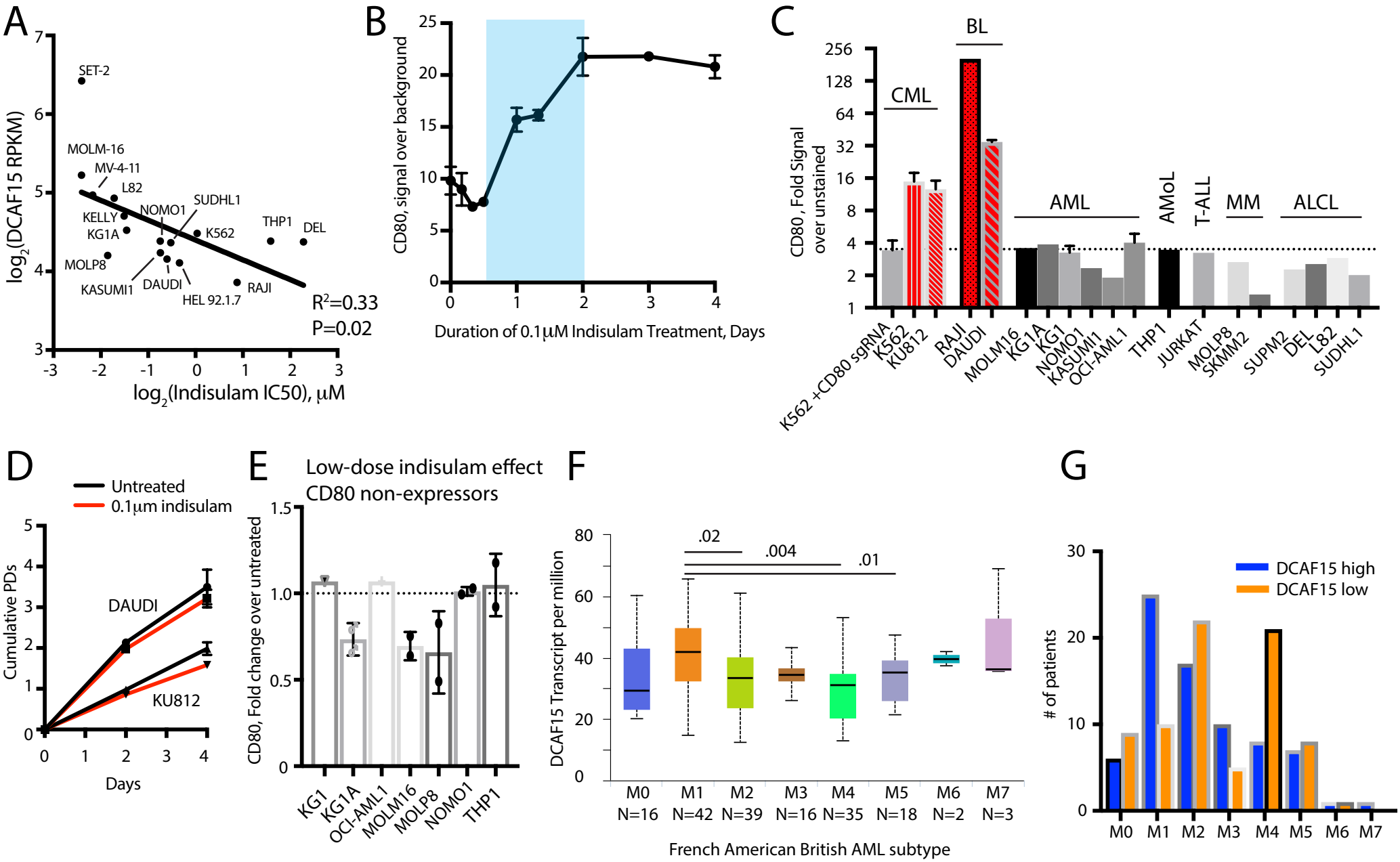
A
log2(DCAF15 RPKM)
log2(Indisulam IC50), μM
SET-2
MOLM-16
MV-4-11
L82
KELLY
NOMO1
SUDHL1
KG1A
K562
THP1
DEL
MOLP8
KASUMI1
DAUDI
HEL 92.1.7
RAJI
R2=0.33
P=0.02
B
CD80, signal over background
Duration of 0.1μM Indisulam Treatment, Days
C
CD80 , Fold Signal over unstained
CML
BL
AML
AMoL
T-ALL
MM
ALCL
K562 +CD80 sgRNA
K562
KU812
RAJI
DAUDI
MOLM16
KG1A
KG1
NOMO1
KASUMI1
OCI-AML1
THP1
JURKAT
MOLP8
SKMM2
SUPM2
DEL
L82
SUDHL1
D
Untreated
0.1μm indisulam
Cumulative PDs
DAUDI
KU812
Days
E
Low-dose indisulam effect
CD80 non-expressors
CD80, Fold change over untreated
KG1
KG1A
OCI-AML1
MOLM16
MOLP8
NOMO1
THP1
F
DCAF15 Transcript per million
.02
.004
.01
M0 N=16
M1 N=42
M2 N=39
M3 N=16
M4 N=35
M5 N=18
M6 N=2
M7 N=3
French American British AML subtype
G
DCAF15 high
DCAF15 low
# of patients
M0
M1
M2
M3
M4
M5
M6
M7

Fig.6-S1

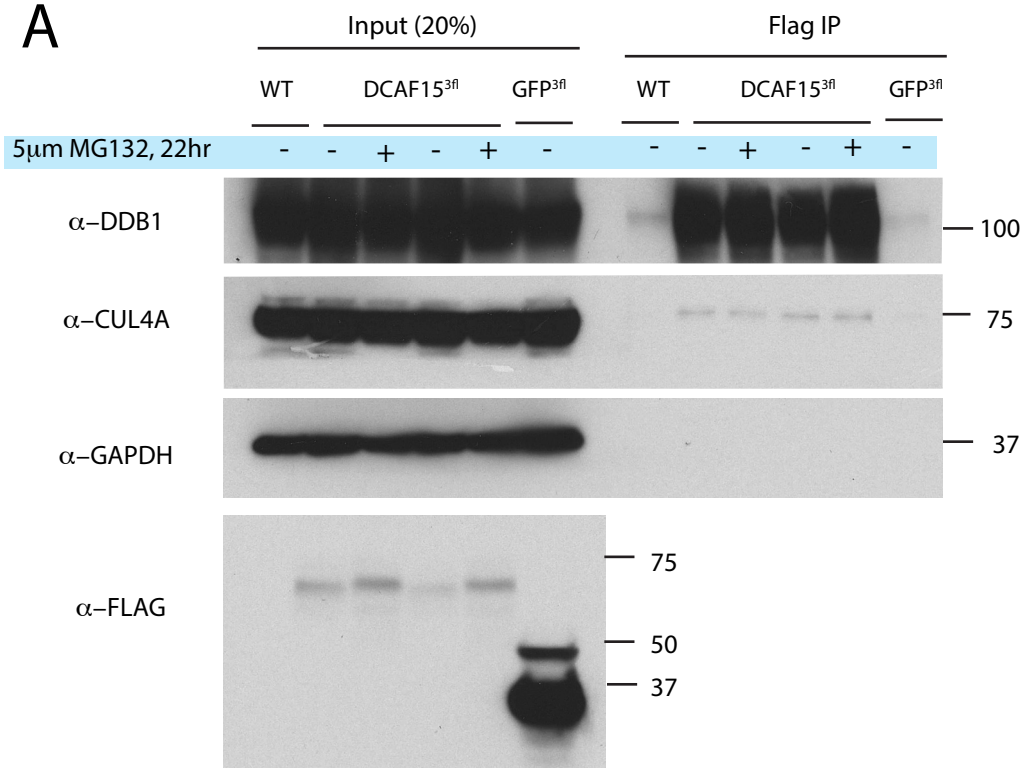

Fig.7-S1